nature cell biology

A SNX3-dependent retromer pathway mediates retrograde transport of the Wnt sorting receptor Wntless and is required for Wnt secretion

Martin Harterink[1], Fillip Port[2,4], Magdalena J. Lorenowicz[1,4], Ian J. McGough[3,4], Marie Silhankova[1,5], Marco C. Betist[1], Jan R. T. van Weering[3], Roy G. H. P. van Heesbeen[1], Teije C. Middelkoop[1], Konrad Basler[2], Peter J. Cullen[3,6,7] and Hendrik C. Korswagen[1,6,7]

Wnt proteins are lipid-modified glycoproteins that play a central role in development, adult tissue homeostasis and disease. Secretion of Wnt proteins is mediated by the Wnt-binding protein Wntless (Wls), which transports Wnt from the Golgi network to the cell surface for release. It has recently been shown that recycling of Wls through a retromer-dependent endosome-to-Golgi trafficking pathway is required for efficient Wnt secretion, but the mechanism of this retrograde transport pathway is poorly understood. Here, we report that Wls recycling is mediated through a retromer pathway that is independent of the retromer sorting nexins SNX1–SNX2 and SNX5–SNX6. We have found that the unrelated sorting nexin, SNX3, has an evolutionarily conserved function in Wls recycling and Wnt secretion and show that SNX3 interacts directly with the cargo-selective subcomplex of the retromer to sort Wls into a morphologically distinct retrieval pathway. These results demonstrate that SNX3 is part of an alternative retromer pathway that functionally separates the retrograde transport of Wls from other retromer cargo.

The classical retromer complex consists of a membrane-bound coat formed by the sorting nexins SNX1–SNX2 and SNX5–SNX6 (referred to as SNX–BAR sorting nexins)[1–4] and a cargo-selective subcomplex consisting of the subunits VPS26, VPS29 and VPS35 (refs 5,6), which binds to a sorting motif in the cytoplasmic tail of cargo proteins[7]. The SNX–BAR sorting nexins are recruited to cargo-containing endosomes through a phosphatidylinositol 3-monophosphate (PtdIns(3)P)-binding Phox homology (PX) domain, and use the carboxy-terminal Bin–amphiphysin–Rvs (BAR) domain to drive membrane deformation and to generate membrane tubules. In recruiting the cargo-selective subcomplex to the forming tubules, the SNX–BAR coat complex is thought to traffic cargo into a tubular-based endosomal sorting pathway[8]. One of the principal functions of this pathway is to mediate retrograde transport between endosomes and the *trans*-Golgi network (TGN), as has been established for cargo proteins such as Vps10p in yeast[9] and the cation-independent mannose 6-phosphate receptor (CI-MPR) in mammals[7,10,11]. It has recently been shown that Wls (also known as Evi or Sprinter)[12–14] is also a retromer cargo[15–19]. Wls binds to the cargo-selective subcomplex, and in mutants of the cargo-selective subunits Wls is missorted and degraded in lysosomes, leading to a strong defect in Wnt secretion and downstream signalling[15–19].

To further examine the function of the retromer complex in the Wnt secretion pathway, we studied the function of the SNX–BAR coat components in Wls recycling. We made the surprising discovery that the SNX–BAR sorting nexins, which are required for the retromer-dependent trafficking of all retromer cargo proteins that have been studied so far[1,6,20–22], are fully dispensable for Wls recycling and Wnt secretion. We show that the unrelated sorting nexin, SNX3, has an evolutionarily conserved function in the Wnt secretion pathway. SNX3 directly interacts with the cargo-selective subunits of the retromer in a complex that does not contain the SNX–BAR coat components. Furthermore, we show that the SNX3 retromer pathway sorts Wls into a retrieval pathway that is morphologically distinct from the SNX–BAR retromer pathway. Our results demonstrate that Wls recycling is mediated by a retromer pathway that separates the recycling of Wls from cargo proteins that take the classical SNX–BAR dependent retromer pathway. We propose that such uncoupling may be essential to achieve the tight regulation of Wnt secretion that is necessary for normal development and adult tissue homeostasis.

[1]Hubrecht Institute, Royal Netherlands Academy of Arts and Sciences and University Medical Center Utrecht, Uppsalalaan 8, 3584 CT, Utrecht, The Netherlands. [2]Institute of Molecular Life Sciences, University of Zurich, Winterthurerstrasse 190, CH-8057 Zurich, Switzerland. [3]Henry Wellcome Integrated Signaling Laboratories, Department of Biochemistry, School of Medical Sciences, University of Bristol, Bristol BS8 1TD, UK. [4]These authors contributed equally to this work. [5]Present address: Department of Cell Biology, Faculty of Science, Charles University Prague, Vinicna 7, 128 00 Prague 2, Czech Republic. [6]Joint senior authors. [7]Correspondence should be addressed to P.J.C. or H.C.K. (e-mail: pete.cullen@bristol.ac.uk or r.korswagen@hubrecht.eu)

Received 23 September 2010; accepted 17 May 2011; published online 3 July 2011; DOI: 10.1038/ncb2281

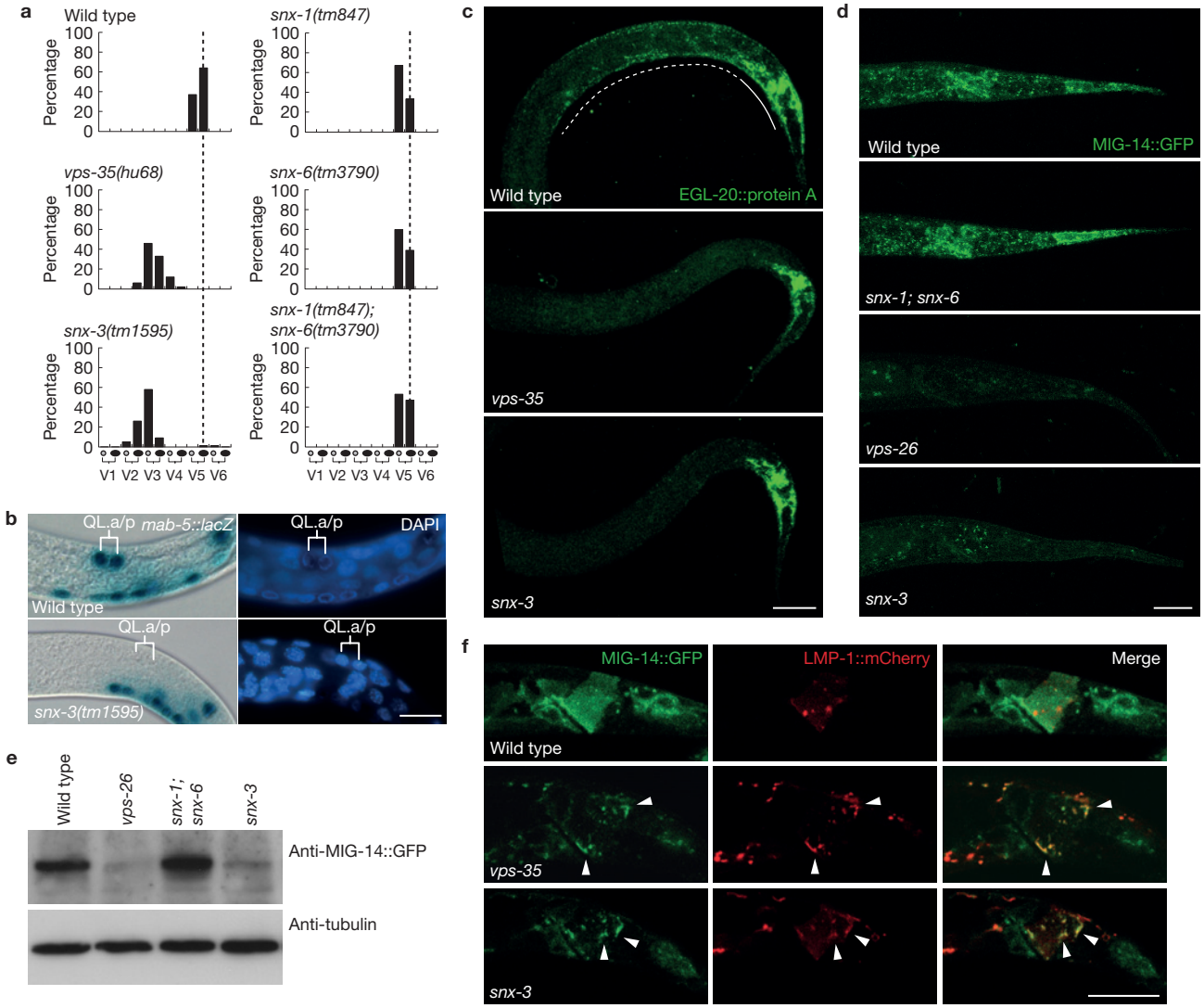

Figure 1 SNX3 is required for EGL-20 (Wnt) signalling and MIG-14 (Wls) recycling in *C. elegans*. (**a**) The final positions of the QL.paa and QL.pap cells relative to the invariant positions of the seam cells V1–V6 ($n > 100$). Both *snx-1(tm847)* and *snx-6(tm3790)* are viable as single or double mutants and could be propagated as homozygous strains, excluding a contribution of maternally provided protein in our assays. (**b**) Expression of the EGL-20 target gene *mab-5* in the QL descendants QL.a and QL.p. Cell nuclei are shown by 4,6-diamidino-2-phenylindole (DAPI) staining. The scale bar is 10 μm. (**c**) Staining of EGL-20::protein A with rabbit anti-goat-Cy5 (ref. 23) in wild type, *vps-35(hu68)* and *snx-3(tm1595)*. Expression is visible within the *egl-20*-expressing cells (solid line) and as a punctate posterior-to-anterior gradient (dotted line). In all images, anterior is to the left and dorsal is up. The scale bar is 10 μm. (**d**) Confocal microscopy images of MIG-14::GFP (*huSi2*) at identical exposure settings in wild type and in *snx-1(tm847); snx-6(tm3790)*, *vps-26(tm1523)* and *snx-3(tm1595)*. The scale bar is 10 μm. (**e**) Western blot quantification of MIG-14::GFP (*huSi2*) protein levels. (**f**) Confocal images of MIG-14::GFP (*huIs71*) (green) and LMP-1::mCherry (red) in wild type, *vps-35(hu68)* and *snx-3(tm1595)*. The arrowheads indicate examples of co-localization between MIG-14::GFP and LMP-1::mCherry. The scale bar is 10 μm. Uncropped images of blots are shown in Supplementary Fig. S7.

RESULTS

The SNX–BAR retromer sorting nexins are dispensable for Wls recycling and Wnt signalling in *Caenorhabditis elegans* and *Drosophila*

In *C. elegans*, mutation of the cargo-selective subunits of the retromer induces defects in several Wnt-dependent processes[23,24], including the EGL-20 (Wnt)-dependent posterior migration of the left Q neuroblast descendants (QL.d). In contrast, we found that mutation of the single SNX1–SNX2 orthologue *snx-1* (ref. 23) and the single SNX5–SNX6 orthologue *snx-6* (ref. 25) did not induce defects in QL.d positioning (Fig. 1a). A comprehensive analysis of other Wnt-dependent processes did not reveal defects either (Supplementary Fig. S1d and Table S1), indicating that *snx-1* and *snx-6* are not required for Wnt signalling in *C. elegans*. Consistently, we found that *snx-1* and *snx-6* are dispensable for the retromer-dependent recycling of the *C. elegans* Wls orthologue MIG-14 (Fig. 1d). In contrast, recycling of the retromer cargo protein CED-1 was fully dependent on *snx-1* and *snx-6* (Supplementary Fig. S2c; ref. 25).

To extend these observations, we knocked down the single SNX5–SNX6 orthologue *Dsnx6* in the posterior compartment of the

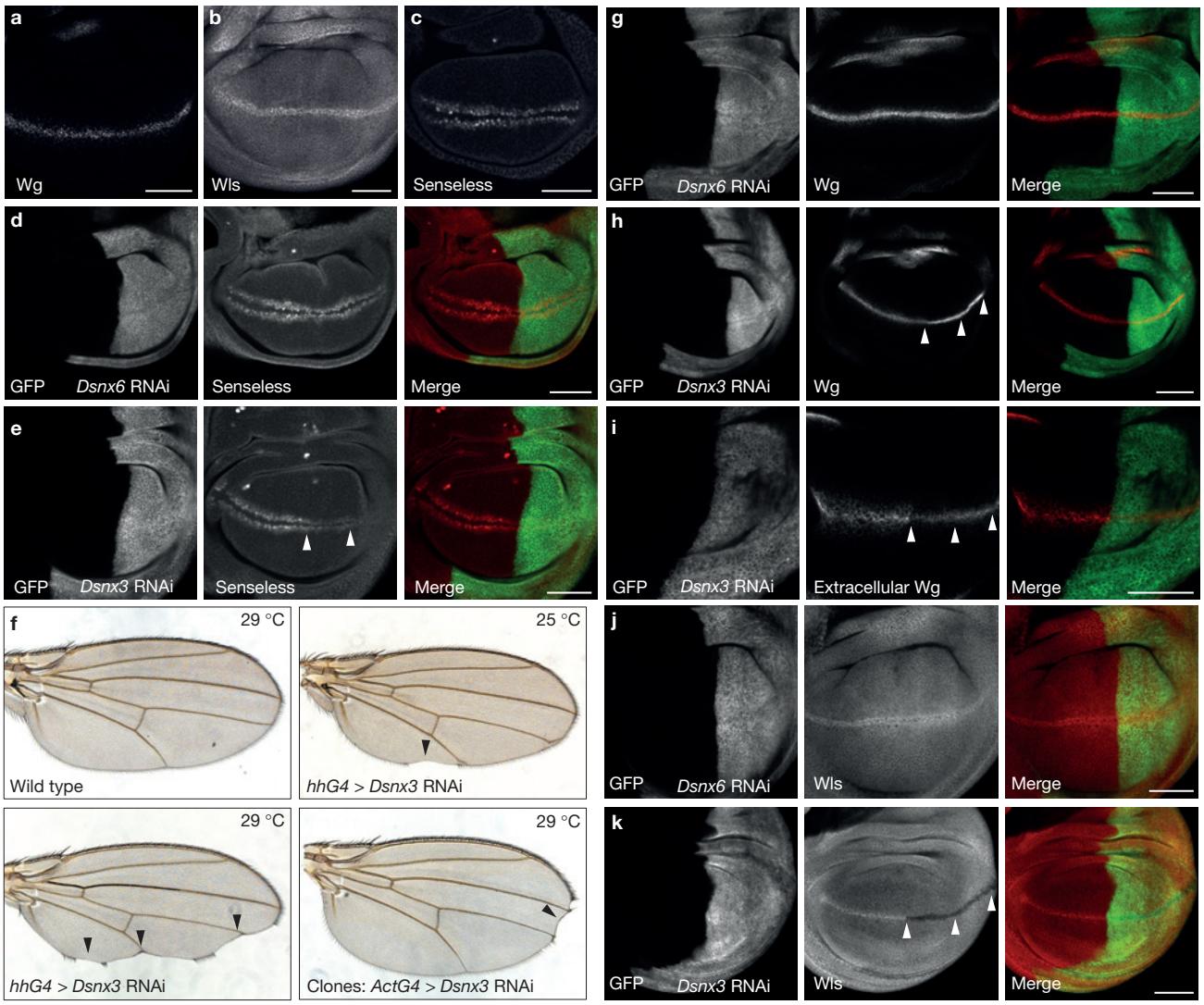

Figure 2 DSnx3 is required for Wg secretion and Wls recycling in the *Drosophila* wing imaginal disc. (**a**–**c**) Immunostaining of Wg, Wls and Senseless in wild-type wing disc. (**d**,**e**,**g**–**k**) Expression of *Dsnx6* or *Dsnx3* RNAi transgenes was induced in the posterior compartment of the wing disc (marked by mCD8–GFP in green) using an *hhGal4* driver (see Supplementary Fig. S3a,b for quantification of knockdown efficiency). (**d**,**e**) Immunostaining of Senseless (red). The arrowheads indicate loss of *senseless* expression in the *Dsnx3* RNAi-expressing posterior compartment. (**f**) *Dsnx3* RNAi was induced in the posterior compartment using *hhGal4* or in clones using an *actinGal4* driver. The arrowheads indicate notches and loss of sensory bristles. (**g**,**h**) Immunostaining of total Wg (red). The arrowheads indicate Wg accumulation in the *Dsnx3* RNAi-expressing posterior compartment. (**i**) Immunostaining of extracellular Wg (red). The arrowheads indicate loss of extracellular Wg staining. (**j**,**k**) Immunostaining of Wls (red). The arrowheads indicate loss of Wls in *wg*-expressing cells in the *Dsnx3* RNAi-expressing posterior compartment. Scale bars, 50 μm.

Drosophila wing imaginal disc by transgene-mediated RNA interference (RNAi). The wing pouch is patterned along the dorsoventral axis by the Wnt protein Wingless (Wg; ref. 26), which is expressed by cells that are located at the dorsoventral boundary of the disc (Fig. 2a). In the absence of Dvps35, Wg secretion is strongly reduced, resulting in accumulation of Wg in the producing cells and a loss of expression of the Wg target gene *senseless* (refs 15,16,18). We found that knockdown of *Dsnx6* did not induce accumulation of Wg (Fig. 2g) and that it also did not reduce the expression of *senseless* (Fig. 2d). Furthermore, knockdown of *Dsnx6* did not affect the levels of endogenous Wls (Fig. 2j), whereas, in the absence of Dvps35, Wls levels are strongly reduced in Wg-producing cells[15,16,18]. Taken together, we conclude that the *C. elegans* and *Drosophila* SNX–BAR orthologues are dispensable for Wls trafficking and Wnt signalling. To our knowledge this is the first example of the cargo-selective subcomplex of the retromer functioning independently of the SNX–BAR retromer sorting nexins.

The PX domain-only sorting nexin SNX3 is required for Wnt signalling

In a genome-wide RNAi screen in *C. elegans* (Supplementary Table S2), we found that the PX domain-only sorting nexin encoded by *snx-3*, which is closely related to yeast Grd19p, *Drosophila* DSnx3 and vertebrate SNX3 and SNX12 (Supplementary Fig. S1b; ref. 8), is

required for the EGL-20 (Wnt)-dependent posterior migration of the QL.d, a result that we confirmed using the predicted *snx-3* null allele *tm1595* (Fig. 1a, Supplementary Fig. S1c). EGL-20 induces posterior migration of the QL.d by activating the target gene *mab-5* (refs 27,28). In *snx-3(tm1595)* mutants, *mab-5* expression was lost in the QL lineage (Fig. 1b), consistent with the notion that *snx-3* is required for the EGL-20-dependent activation of *mab-5*. This conclusion is supported by the rescue of the QL.d migration defect of *snx-3* by EGL-20-independent activation of *mab-5*. Thus, the QL.d localize at their normal posterior positions in double mutants between *snx-3* and the *mab-5* gain-of-function allele *e1751* (ref. 28) and in double mutants with the Axin orthologue *pry-1* (Supplementary Table S3; refs 29,30). In addition to the defect in QL.d migration, *snx-3(tm1595)* showed a range of other Wnt-related phenotypes. Thus, the final position of the QR.d and the hermaphrodite-specific neurons (HSNs) was shifted towards the posterior and the polarity of the anterior and posterior lateral mechanosensory (ALM and PLM respectively) neurons was lost or reversed (Supplementary Table S1 and Fig. S1d). Taken together, these results show that *snx-3* is required for several Wnt-dependent processes and that the range and penetrance of these phenotypes are similar to those of mutations in components of the cargo-selective retromer subcomplex[23,24].

To investigate whether SNX3 is required for Wnt signalling in *Drosophila*, we knocked down the single SNX3 orthologue *Dsnx3* in the posterior compartment of the wing imaginal disc. As shown in Fig. 2e, there was a strong reduction in expression of the high-threshold Wg target gene *senseless*. Furthermore, knockdown of *Dsnx3* in the posterior compartment or in clones frequently resulted in typical *wg* loss-of-function defects in the adult wing, such as notches and a loss of sensory bristles at the wing periphery (Fig. 2f). These results establish that SNX3 has an evolutionarily conserved function in Wnt signalling.

SNX3 is required in Wnt-producing cells for Wnt secretion

We found that *snx-3* is ubiquitously expressed in *C. elegans*, with prominent expression in coelomocytes, the pharynx and rectal epithelial cells, which include the cells that produce and secrete EGL-20 (Supplementary Fig. S2a). We have previously shown that the cargo-selective subcomplex of the retromer is specifically required in Wnt-producing cells[23]. To investigate whether *snx-3* has a similar site of action, we tested whether specific expression of wild-type *snx-3* in the EGL-20-producing cells of *snx-3(tm1595)* mutants restores the EGL-20-dependent posterior migration of the QL.d. We found that *egl-20* promoter-directed expression of *snx-3* significantly rescued QL.d migration (Supplementary Table S3). In contrast, expression of *snx-1* did not restore QL.d migration. We conclude that the presence of *snx-3* in Wnt-producing cells is necessary and sufficient for its function in Wnt signalling. Furthermore, these results show that *snx-3* and the cargo-selective retromer subcomplex not only produce similar mutant phenotypes, but also share a common site of action.

The requirement of *snx-3* in Wnt-producing cells suggests a function of SNX3 in Wnt secretion. To investigate this possibility, we tested whether the secretion of EGL-20 is affected in *snx-3* mutants. EGL-20 (visualized using the immunoglobulin-binding domain of protein A as a tag) forms a punctate concentration gradient that ranges from the *egl-20*-expressing cells in the tail to the mid-body region (Fig. 1c; ref. 23). In *vps-35* mutants, this gradient is strongly reduced or absent. We found that the EGL-20 gradient was similarly reduced in *snx-3(tm1595)* (Fig. 1c), indicating that *snx-3* is necessary for EGL-20 secretion. To determine whether DSnx3 is also required for Wnt secretion and gradient formation in *Drosophila*, we depleted *Dsnx3* in the posterior compartment of the wing imaginal disc and stained for endogenous Wg. As shown in Fig. 2h and Supplementary Fig. S3c,d, knockdown or mutation of *Dsnx3* resulted in a strong accumulation of Wg within the stripe of *wg*-expressing cells along the dorsoventral boundary, indicating that Wg secretion is strongly reduced. Indeed, staining of extracellular Wg showed that there was a strong reduction in the level of Wg outside the *wg*-expressing cells (Fig. 2i). Taken together, these results are consistent with a conserved function of SNX3 in Wnt secretion.

To address the specificity of SNX3 for Wnt secretion, we tested whether knockdown of *Dsnx3* affects the secretion of two other morphogens in the wing disc: the lipid-modified Hedgehog (Hh) protein[31] and the *Drosophila* BMP (bone morphogenetic protein) orthologue decapentaplegic (Dpp; ref. 32). Depletion of *Dsnx3* in the dorsal compartment or in large clones spanning the *hh*-expressing domain of the wing imaginal disc did not interfere with Hh secretion, as determined by monitoring endogenous Hh protein (Supplementary Fig. S3d). To examine effects on Dpp secretion, Dpp signalling activity was measured by staining of phosphorylated Mad protein (pMad), a downstream effector in the Dpp pathway[33], but again no effects were observed when *Dsnx3* was depleted (Supplementary Fig. S3e). Although these experiments assay only a limited set of secreted proteins, these results clearly indicate that DSnx3 is not generally required for protein secretion. This conclusion is further supported by the *snx-3* mutant phenotype in *C. elegans*: apart from a defect in Wnt signalling, *snx-3* mutants have no other obvious developmental defects (data not shown).

SNX3 has a conserved function in regulating Wls stability

To examine the function of SNX3 in the Wnt secretion pathway, we tested whether depletion of *snx-3* has an effect on the subcellular localization or stability of MIG-14 (Wls; refs 12–14). As shown in Fig. 1d,e, there was a striking decrease in MIG-14 protein levels in *snx-3(tm1595)*, which was similar to the reduction observed in the cargo-selective subcomplex mutant *vps-26*. In contrast, steady-state levels of the retromer cargo protein CED-1 were not significantly changed in the absence of *snx-3* (Supplementary Fig. S2c). Also in *Drosophila*, depletion of *Dsnx3* resulted in a loss of endogenous Wls protein (Fig. 2k, Supplementary Fig. S3c,d). Interestingly, Wls levels were only reduced within the *wg*-expressing cells, an effect that was also observed on knockdown of *Dvps35* (ref. 18). We conclude that SNX3 has a conserved function in maintaining Wls protein levels.

To determine whether the reduction in MIG-14 protein levels is the result of lysosomal degradation, we carried out co-localization studies between MIG-14 and the late endosomal and lysosomal marker LMP-1::mCherry in *C. elegans* (ref. 19). In wild-type animals, no significant co-localization between MIG-14::GFP (green fluorescent protein) and LMP-1::mCherry could be observed in *egl-20*-expressing cells (Fig. 1f). However, in *snx-3(tm1595)* mutants, the remaining MIG-14::GFP was mostly localized to LMP-1::mCherry-positive structures. These results indicate that MIG-14 is missorted into the

lysosomal degradation pathway in *snx-3* mutants, consistent with a function of SNX3 in the retromer-dependent endosome-to-TGN transport of MIG-14.

To investigate whether MIG-14 becomes limiting for Wnt signalling in *snx-3* mutants, we tested whether *mig-14* overexpression can rescue EGL-20 signalling. Overexpression of a functional MIG-14::GFP fusion protein from a multicopy transgene fully rescued the QL.d migration defect of *snx-3(tm1595)* (Supplementary Table S3), supporting the hypothesis that the Wnt secretion defect of *snx-3* mutants is caused by a decrease in MIG-14 (Wls) protein level.

Human SNX3 co-localizes with Wls and VPS26 on endosomes and facilitates membrane association of the cargo-selective retromer subcomplex

To investigate how SNX3 and the cargo-selective subcomplex functionally interact in Wls recycling, we examined human SNX3 in HeLa cells, which express SNX3 but lack detectable expression of the related sorting nexin SNX12 (Supplementary Fig. S4a,b). Using a lentivirally expressed GFP–SNX3 fusion protein, we found that SNX3 co-localizes with the cargo-selective retromer subunit VPS26 on endosomes (Fig. 3a), as was confirmed by immuno-electron microscopy (Fig. 3b). Furthermore, we found that GFP–SNX3 co-localizes with Wls–mCherry (Fig. 4a, and Supplementary Fig. S2b for co-localization in *C. elegans*). Knockdown of SNX3 led to a significant reduction in endogenous human Wls protein levels (Fig. 4d), consistent with the conserved function of SNX3 in maintaining Wls protein levels. SNX3 depletion also induced a striking reduction in co-localization between Wls–mCherry and endogenous VPS26 (Fig. 4b,c). As the VPS26 staining pattern seemed more cytoplasmic than in control siRNA-treated cells, we tested whether SNX3 is required for membrane association of VPS26. Similar to knockdown of RAB7, which has been shown to mediate membrane recruitment of the cargo-selective subcomplex to late endosomes[34,35], depletion of SNX3 induced a decrease in membrane-associated VPS26 and a corresponding increase in cytoplasmically localized VPS26 (Fig. 4e). These results are consistent with a function of SNX3 in aiding the association of the cargo-selective subunits to Wls-containing endosomes. Whether this function is independent of other retromer recruitment mechanisms, such as mediated by RAB7 (refs 34,35) and Hrs (ref. 36), remains to be established.

SNX3 physically interacts with the cargo-selective retromer subunits in a complex that does not contain the SNX–BAR sorting nexins

To investigate whether SNX3 and the retromer physically interact, we carried out co-immunoprecipitation experiments with GFP–SNX3. As shown in Fig. 3c, there was significant co-immunoprecipitation between SNX3 and both endogenous VPS35 and VPS26, indicating that SNX3 and the cargo-selective retromer subcomplex can associate *in vivo*. This interaction is direct, as recombinant full-length SNX3 co-precipitated with purified VPS26–VPS29–VPS35 trimeric complex (Fig. 3d and Supplementary Fig. S4c). Next, we compared immunoprecipitates of SNX3 with immunoprecipitates of the SNX–BAR sorting nexins SNX1 and SNX5 (Fig. 3c). Although in both cases the cargo-selective subunits were co-precipitated (note however that the interaction with SNX1–SNX5 is weaker than with SNX3), we failed to detect endogenous SNX1 and SNX5 in the SNX3 immunoprecipitate and endogenous SNX3 in the SNX1 and SNX5 immunoprecipitate. On the basis of these results, we conclude that there are two distinct retromer complexes: a SNX–BAR-containing retromer complex, and a complex in which SNX3 interacts with the cargo-selective retromer subcomplex.

SNX3 localizes to early endosomes and segregates Wls into a retrieval pathway that is morphologically distinct from the SNX–BAR retromer pathway

To examine the spatial distribution of SNX3 and the SNX–BAR sorting nexins along the endosomal maturation pathway, we expressed GFP–SNX3 and GFP–SNX1 in HeLa cells. Using markers for early (EEA1 and RAB5) and late endosomes and lysosomes (LAMP1 and RAB7), we found that GFP–SNX3 primarily localizes to early endosomes (Fig. 3a), in agreement with the previously reported localization of SNX3 in A431 cells[37]. In contrast, the classical SNX–BAR retromer sorting nexins are most abundant on endosomes that are at the early-to-late endosomal transition point[22] (J.R.T. van Weering and P.J. Cullen, unpublished observations). Consistent with this distinct but overlapping distribution, co-localization between SNX1 and SNX3 was only partial (Fig. 3a), supporting the notion that SNX3 and SNX1 show an element of spatial segregation along the endosomal maturation pathway.

The SNX–BAR retromer sorting nexins contain a membrane-curvature-sensing BAR domain, which drives membrane deformation to segregate cargo into a tubular-based endosomal trafficking pathway[8]. SNX3 lacks a BAR domain, indicating that it may direct Wls and the cargo-selective retromer subcomplex into a morphologically distinct sorting pathway. Using live-cell confocal microscopy imaging to define the dynamic relationship between SNX3, the SNX–BAR sorting nexins and Wls, we found that Wls is not sorted into SNX–BAR-labelled tubular endosomal profiles. Thus, in cells expressing GFP–SNX1 and Wls–mCherry, Wls was not enriched in SNX1-decorated tubules emerging from endosomes labelled for both proteins (Fig. 5a,b and Supplementary Fig. S4d) (18/22 tubules were negative for Wls, whereas 4/22 were weakly positive). Instead, we observed the emergence of small GFP–SNX3- and Wls–mCherry-labelled transport vesicles from endosomes co-labelled for both proteins (Fig. 5c). These results are consistent with our observation that the SNX–BAR sorting nexins are dispensable for Wls trafficking and indicate that Wls exits SNX3-labelled early endosomes through vesicular carriers rather than through SNX–BAR-decorated tubular profiles. This conclusion is further supported by the observation that SNX3 interacts with clathrin[38], a result that we have confirmed here through endogenous co-immunoprecipitation (Supplementary Fig. S5a). Although SNX3 has been suggested to contain an inverted clathrin box[38], the interaction seems indirect, as recombinant SNX3 did not associate with recombinant clathrin (residues 1–579) in either the absence or presence of PtdIns(3)P-containing liposomes (Supplementary Fig. S5b,c). Immunostaining of endogenous clathrin revealed that a small population of SNX3-decorated endosomes co-localizes with clathrin (Supplementary Fig. S5d). At the resolution of immuno-electron microscopy, these appear as clathrin-coated, small 50–75 nm vesicles

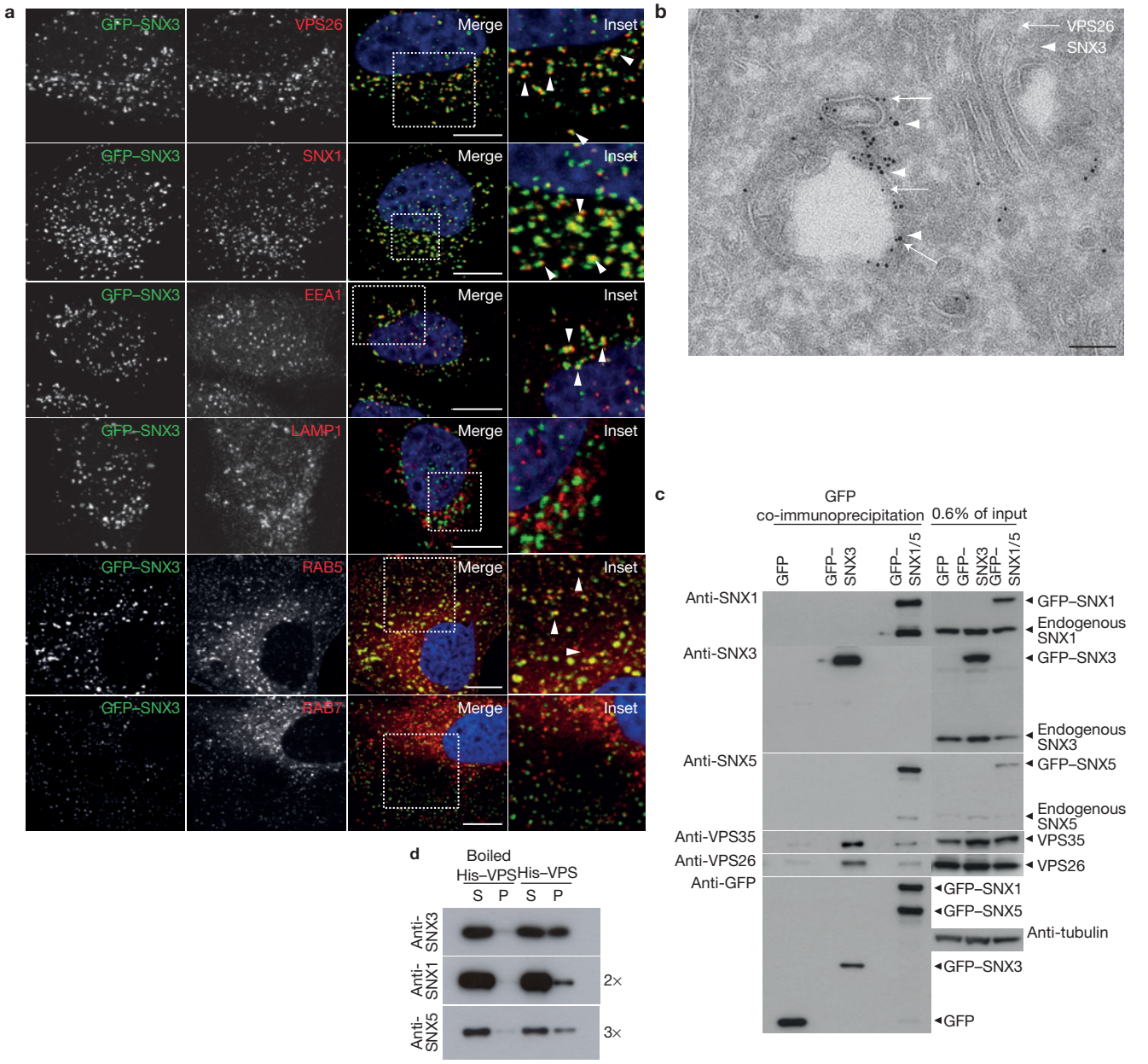

Figure 3 Co-localization and physical interaction of SNX3 with the cargo-selective subcomplex of the retromer. (**a**) SNX3 partially co-localizes with VPS26-positive early endosomes. HeLa cells lentivirally transduced to express GFP–SNX3 (green) were fixed and stained for VPS26, SNX1, EEA1 or LAMP1 (red). Co-localization between GFP–SNX3 and VPS26, SNX1, EEA1, LAMP1, RAB5–mCherry and RAB7–mCherry was quantified as 0.43 ± 0.05, 0.55 ± 0.04, 0.38 ± 0.02, 0.07 ± 0.04, 0.61 ± 0.02 and 0.34 ± 0.02, respectively (Pearson's coefficient, mean $\pm$ s.d., $n = 3$ with 30 cells per condition; for RAB5 and RAB7, $n = 20$ cells). Scale bar, 11 μm. (**b**) At the ultrastructural level, SNX3 and VPS26 localize to common vesicular endosomal profiles. GFP–SNX3 is labelled with 10 nm gold and mCherry–VPS26 with 6 nm gold. The image is representative of that observed from the analysis of five other endosomal vacuoles. Scale bar, 100 nm. (**c**) SNX3 interacts with the cargo-selective subcomplex of the retromer. Cell extracts derived from HeLa cells lentivirally transduced with GFP, GFP–SNX3 or both GFP–SNX1 and GFP–SNX5 (GFP–SNX1/5) were subjected to a GFP nanotrap. The classical retromer SNX–BARs form heterodimeric complexes, leading to the presence of both endogenous SNX1 and SNX5 in the GFP–SNX1/5 immunoprecipitates[3]. (**d**) 3xFlag–VPS26–VPS29–VPS35–His_6 complex (His–VPS) was isolated from BL21 *Escherichia coli* onto TALON resin and incubated with 2 μM of recombinant SNX3, SNX1 or SNX5 for 2 h at 4 °C. Supernatant (S) and TALON-containing resin (P) were isolated. SNX3 directly associates with His–VPS, as do SNX1 and SNX5 although this is less well pronounced (longer exposures are shown; 2× and 3×). Control: boiled His–VPS resin. Uncropped images of blots are shown in Supplementary Fig. S8.

(Supplementary Fig. S5e) that are morphologically distinct from the previously characterized retromer-decorated endosome-to-TGN transport carriers, which appear as clathrin-negative, non-branched tubules (average length 170–230 nm and diameter 20–50 nm)[22]. These results suggest that SNX3 may direct the Wls–retromer complex into a clathrin-dependent vesicular transport pathway. Future studies will examine how Wls trafficking is mediated by the SNX3 retromer complex.

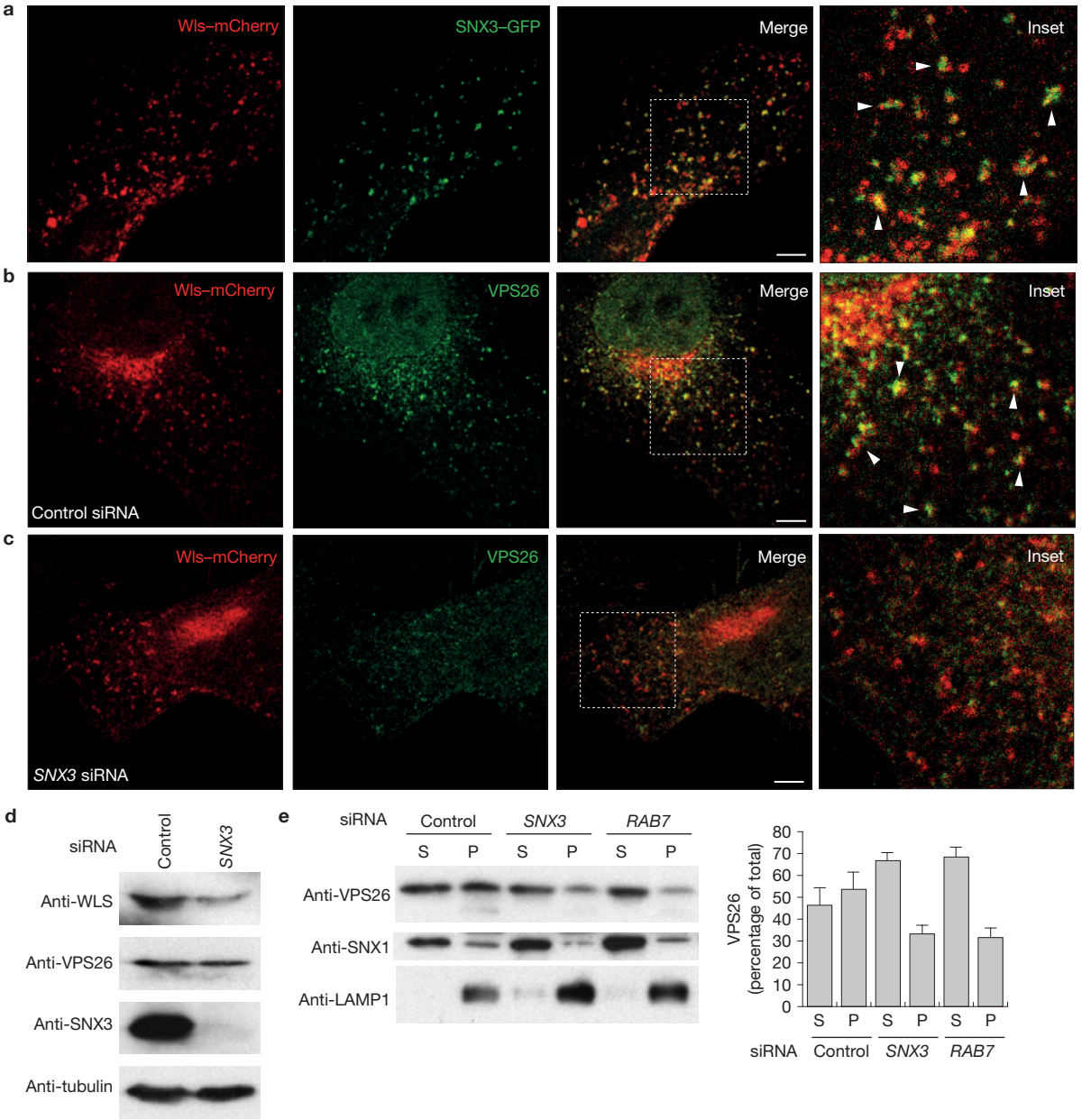

Figure 4 SNX3 co-localizes with Wls and facilitates membrane association of the cargo-selective subcomplex of the retromer. (**a**) Co-localization between SNX3–GFP (green) and Wls–mCherry (red) in HeLa cells was quantified as 0.25 ± 0.02 (Pearson's coefficient; mean ± s.e.m., $n = 2$ with 23 and 11 cells). The arrowheads show examples of co-localization. Scale bar, 10 μm. (**b**,**c**) Co-localization between Wls–mCherry and endogenous VPS26 (green) in HeLa cells treated with control or *SNX3* siRNA was quantified as 0.19 ± 0.02 and 0.08 ± 0.02, respectively (Pearson's coefficient; mean ± s.e.m., $n = 4$ with seven to ten cells each). The arrowheads show examples of co-localization. (**d**) HeLa cells were transfected with control or *SNX3* siRNA and assayed for endogenous Wls, VPS26, SNX3 and tubulin protein levels. (**e**) HeLa cells treated with control, *SNX3* or *RAB7* siRNA were separated into a supernatant (S) fraction containing cytosol and a pellet fraction (P) containing membranes[34] and were stained for endogenous VPS26, SNX1 and LAMP1. The amount of VPS26 in the supernatant and pellet fractions was quantified using densitometry and is shown as a percentage of the total. Data are presented as mean ± s.e.m. and represent three independent experiments. There was no significant change in SNX1 membrane association on SNX3 knockdown (17.8 ± 3.1% in control versus 22 ± 6.6% in SNX3 knockdown; data are means ± s.e.m., $n = 3$, $P > 0.5$ Student's *t*-test). Knockdown of RAB7 was included as a positive control[34]. Uncropped images of blots are shown in Supplementary Fig. S9.

DISCUSSION

The identification of the Wnt sorting receptor Wls has shown that the secretion of Wnt proteins is mediated by a specialized trafficking pathway that provides an important layer of regulation to Wnt signalling[39,40]. A key step in this pathway is the retromer-dependent transport of Wls from endosomes to the TGN (refs 15–19). Here, we report that Wls retrieval is mediated by a retromer pathway that functions independently of the SNX–BAR retromer coat components.

The retromer consists of a cargo-selective subcomplex that interacts with sorting nexins of the SNX–BAR family to segregate cargo into

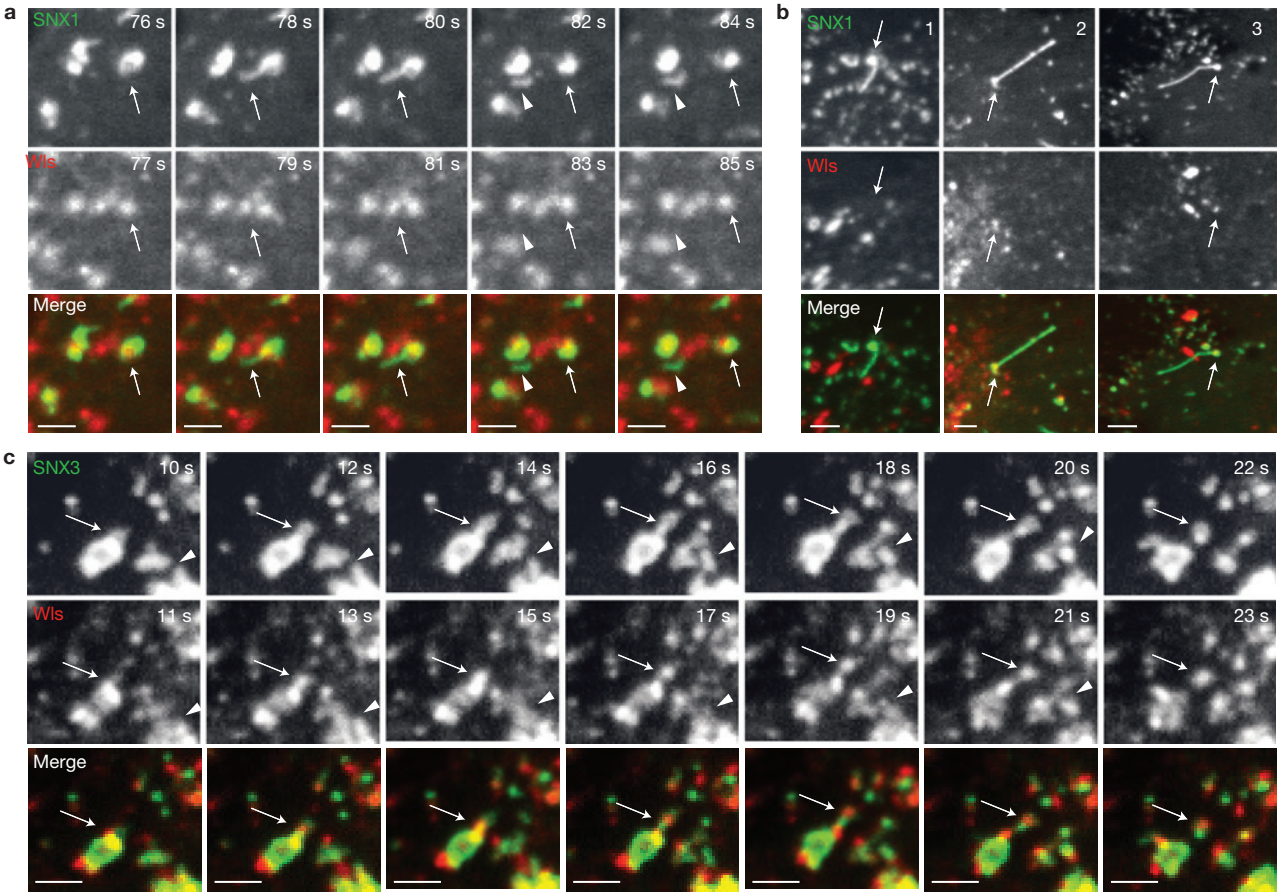

Figure 5 Wls is contained within SNX3-positive vesicular carriers but is absent from SNX1 retromer-decorated tubular carriers. (**a**) RPE-1 cells were transiently co-transfected with pEGFP–SNX1 (green) and Wls–mCherry (red) and cells were subsequently imaged live after a 16 h incubation period. Frames depicting the formation and scission of a GFP–SNX1 tubule from a vesicle positive for both SNX1 and Wls are shown (the arrows indicate the dual-expressing vesicle, whereas the arrowheads indicate the carrier post scission) (see Supplementary Movie S1). Scale bars represent 6 μm. Of the 100 SNX1-decorated tubulating endosomes that were analysed, 22 were positive for Wls; 18/22 tubules emanating from these endosomes were negative for Wls, whereas 4/22 were weakly positive. Quantification of Wls–mCherry and GFP–SNX1 levels in an endosome and corresponding tubule is shown in Supplementary Fig. S4d. (**b**) Further examples of SNX1 retromer tubules negative for Wls. (1) An example of a SNX1 retromer-positive endosome and tubule both of which are negative for Wls. (2,3) Further examples of SNX1-labelled endosomes positive for Wls, but with tubules negative for Wls. Scale bars represent 6 μm. (**c**) RPE-1 cells were transiently co-transfected with pEGFP–SNX3 (green) and Wls–mCherry (red) and cells were subsequently imaged live after a 16 h incubation period. Frames depicting the formation and scission of GFP–SNX3-labelled buds from vesicles positive for both SNX3 and Wls are shown. Note the 1 s delay between acquisitions for a given image pair. The arrows and arrowheads show two examples of buds positive for both Wls and SNX3 (see Supplementary Movie S2). Scale bars represent 6 μm.

a tubular endosomal sorting pathway[8]. Our results show that the cargo-selective subcomplex also interacts with SNX3 as part of an alternative retromer pathway that mediates the recycling of Wls. Three lines of evidence suggest that these are functionally distinct retromer pathways. First, genetic analysis in *C. elegans* showed that *snx-3* and the SNX–BAR sorting nexins function in parallel pathways. Thus, retrieval of the phagocytic receptor CED-1 (ref. 25) is dependent on the SNX–BAR sorting nexins but independent of SNX3, whereas Wls recycling requires SNX3 but not the SNX–BAR sorting nexins. Second, co-immunoprecipitation experiments showed that the interaction of the cargo-selective subcomplex of the retromer with the SNX–BAR sorting nexins and SNX3 is mutually exclusive. Finally, live-cell imaging revealed that the SNX3 retromer pathway sorts Wls into a vesicular retrieval pathway that is morphologically distinct from the SNX–BAR-dependent tubular endosomal sorting pathway[8]. On the basis of these results we conclude that the SNX–BAR and SNX3 pathways are independent and mechanistically distinct retromer pathways.

Studies in yeast have shown that the SNX3 orthologue Grd19p also functions in retromer-dependent endosome-to-Golgi retrieval[21,41–43], but, in contrast to SNX3, Grd19p functions together with the SNX–BAR sorting nexins Vps5p and Vps17p in the retrieval of cargo proteins such as the iron transporter Fet3p–Ftr1p. Grd19p physically interacts with a sorting sequence in the cytoplasmic tail of Ftr1p and with the SNX–BAR retromer complex, which led to the hypothesis that Grd19p acts as a cargo-specific adaptor that links Ftr1p to the SNX–BAR retromer complex[43]. We did not observe an interaction between SNX3 and Wls in co-immunoprecipitation experiments (data not shown) and also did not find co-precipitation of SNX3 with the SNX–BAR sorting nexins. Furthermore, we found that mutation of the SNX–BAR sorting nexins did not affect the SNX3-dependent retrieval of Wls,

indicating that the function of SNX3 is fundamentally different from that of Grd19p in yeast.

How do the two distinct SNX3- and SNX–BAR-retromer complexes regulate sorting of different endosomal cargo? One simple model to answer this question relies on the spatial segregation of SNX3 and the SNX–BAR sorting nexins along the endosomal maturation pathway. Although there is significant co-localization between these sorting nexins, SNX3 is predominantly localized to early endosomes by its high-affinity interaction with PtdIns(3)P (ref. 44), whereas the SNX–BAR retromer sorting nexins reside at the interface between early and late endosomes[22]. Endocytosed Wls therefore initially enters SNX3-labelled early endosomes, where it engages the VPS26–VPS29–VPS35 trimeric complex, recruited to this compartment by the interaction with SNX3 (Supplementary Fig. S6). Through a vesicular pathway, possibly dependent on indirect binding to clathrin as well as further membrane-remodelling proteins, the SNX3 retromer complex sorts Wls for retrieval to the TGN. In the absence of SNX3, Wls can be missorted into intraluminal vesicles and hence lysosomal degradation, or can be recycled through SNX–BAR retromer to the TGN. The relative flux through these two distinct pathways therefore determines the steady-state level of Wls. As the level of Wls is severely reduced on loss of SNX3, the flux into the lysosomal degradative pathway seems to be dominant. Thus, although a proportion of Wls may undergo SNX–BAR retromer-mediated recycling in the absence of SNX3, this is insufficient to maintain the required level of Wls for Wnt gradient formation during iterative rounds of Wnt secretion and Wls retrieval from the cell surface.

Interestingly, the steady-state trafficking of the classical SNX–BAR retromer cargo CI-MPR is primarily defined by intracellular cycling between the TGN and late endosomes with retrieval to the TGN by way of the SNX–BAR retromer. The spatial-segregation model therefore suggests that the lack of effect of SNX3 suppression on steady-state CI-MPR distribution arises from CI-MPR entering the endosomal network at a point downstream of SNX3 (ref. 3). That said, the complexity of CI-MPR trafficking—a proportion of this receptor traffics to the plasma membrane before undergoing endocytosis and retrograde transport to the TGN (refs 45–47)—suggests that such a simple spatial-segregation model may be an oversimplification. We therefore speculate that, alongside spatial segregation, cargo binding to the VPS26–VPS29–VPS35 complex may be an important element in selecting the sorting nexin coat that specifies the subsequent retrograde trafficking route. Thus, binding of VPS26–VPS29–VPS35 to Wls may favour association with SNX3, whereas engagement with CI-MPR favours binding to the SNX–BAR coat complex. □

METHODS

Methods and any associated references are available in the online version of the paper at http://www.nature.com/naturecellbiology

Note: Supplementary Information is available on the Nature Cell Biology website

ACKNOWLEDGEMENTS

We thank C. Rabouille for critically reading the manuscript, M. Seaman for advice, D. Xue (University of Colorado, Boulder) for *smIs34*, M. Tabuchi (Kawasaki Medical School, Okayama, Japan) for the bacterial construct expressing 3 × Flag-tagged retromer complex, S. Mitani (National Bioresource Project for the Nematode, Tokyo, Japan) for deletion mutants, A. Fire for expression vectors and the *Caenorhabditis* Genetic Center (University of Minnesota, Minneapolis) for strains. This work was funded by the Dutch Cancer Society (HUBR 2008-4114), the EU FP6 Programme Cells into Organs and NWO VIDI (016.076.317) (H.C.K.), an NWO VENI fellowship (M.J.L.), a Boehringer Ingelheim Foundation fellowship (M.H.), the Swiss National Science Foundation and the Forschungskredit of the University of Zürich (F.P. and K.B.) and the Wellcome Trust (089928/Z/09/Z and 085743) (P.J.C.). I.J.M. is a Wellcome Trust-funded PhD student (086777/Z/08/Z).

AUTHOR CONTRIBUTIONS

M.H., M.S., T.C.M., M.C.B., R.G.H.P.H. and H.C.K. designed and carried out the *C. elegans* experiments, F.P. and K.B. designed and carried out the *Drosophila* experiments, M.J.L., I.J.M., J.R.T.W., H.C.K. and P.J.C. designed and carried out the cell biological analysis of SNX3 function in tissue culture cells and M.H., K.B., P.J.C. and H.C.K. wrote the paper.

COMPETING FINANCIAL INTERESTS

The authors declare no competing financial interests.

Published online at http://www.nature.com/naturecellbiology
Reprints and permissions information is available online at http://www.nature.com/reprints

1. Carlton, J. *et al.* Sorting nexin-1 mediates tubular endosome-to-TGN transport through coincidence sensing of high- curvature membranes and 3-phosphoinositides. *Curr. Biol.* **14,** 1791–1800 (2004).
2. Carlton, J. G. *et al.* Sorting nexin-2 is associated with tubular elements of the early endosome, but is not essential for retromer-mediated endosome-to-TGN transport. *J. Cell Sci.* **118,** 4527–4539 (2005).
3. Wassmer, T. *et al.* A loss-of-function screen reveals SNX5 and SNX6 as potential components of the mammalian retromer. *J. Cell Sci.* **120,** 45–54 (2007).
4. Wassmer, T. *et al.* The retromer coat complex coordinates endosomal sorting and dynein-mediated transport, with carrier recognition by the *trans*-Golgi network. *Dev. Cell* **17,** 110–122 (2009).
5. Seaman, M. N. Recycle your receptors with retromer. *Trends Cell Biol.* **15,** 68–75 (2005).
6. Attar, N. & Cullen, P. J. The retromer complex. *Adv. Enzyme Regul.* **50,** 216–236 (2009).
7. Seaman, M. N. Identification of a novel conserved sorting motif required for retromer-mediated endosome-to-TGN retrieval. *J. Cell Sci.* **120,** 2378–2389 (2007).
8. Cullen, P. J. Endosomal sorting and signalling: an emerging role for sorting nexins. *Nat. Rev. Mol. Cell Biol.* **9,** 574–582 (2008).
9. Seaman, M. N., McCaffery, J. M. & Emr, S. D. A membrane coat complex essential for endosome-to-Golgi retrograde transport in yeast. *J. Cell Biol.* **142,** 665–681 (1998).
10. Seaman, M. N. Cargo-selective endosomal sorting for retrieval to the Golgi requires retromer. *J. Cell Biol.* **165,** 111–122 (2004).
11. Arighi, C. N., Hartnell, L. M., Aguilar, R. C., Haft, C. R. & Bonifacino, J. S. Role of the mammalian retromer in sorting of the cation-independent mannose 6-phosphate receptor. *J. Cell Biol.* **165,** 123–133 (2004).
12. Banziger, C. *et al.* Wntless, a conserved membrane protein dedicated to the secretion of Wnt proteins from signaling cells. *Cell* **125,** 509–522 (2006).
13. Bartscherer, K., Pelte, N., Ingelfinger, D. & Boutros, M. Secretion of Wnt ligands requires Evi, a conserved transmembrane protein. *Cell* **125,** 523–533 (2006).
14. Goodman, R. M. *et al.* Sprinter: a novel transmembrane protein required for Wg secretion and signaling. *Development* **133,** 4901–4911 (2006).
15. Belenkaya, T. Y. *et al.* The retromer complex influences Wnt secretion by recycling Wntless from endosomes to the *trans*-Golgi network. *Dev. Cell* **14,** 120–131 (2008).
16. Franch-Marro, X. *et al.* Wingless secretion requires endosome-to-Golgi retrieval of Wntless/Evi/Sprinter by the retromer complex. *Nat. Cell Biol.* **10,** 170–177 (2008).
17. Pan, C. L. *et al. C. elegans* AP-2 and retromer control Wnt signaling by regulating *mig-14*/Wntless. *Dev. Cell* **14,** 132–139 (2008).
18. Port, F. *et al.* Wingless secretion promotes and requires retromer-dependent cycling of Wntless. *Nat. Cell Biol.* **10,** 178–185 (2008).
19. Yang, P. T. *et al.* Wnt signaling requires retromer-dependent recycling of MIG-14/Wntless in Wnt-producing cells. *Dev. Cell* **14,** 140–147 (2008).
20. Nothwehr, S. F. & Hindes, A. E. The yeast VPS5/GRD2 gene encodes a sorting nexin-1-like protein required for localizing membrane proteins to the late Golgi. *J. Cell Sci.* **110 (Pt 9),** 1063–1072 (1997).
21. Hettema, E. H., Lewis, M. J., Black, M. W. & Pelham, H. R. Retromer and the sorting nexins Snx4/41/42 mediate distinct retrieval pathways from yeast endosomes. *EMBO J.* **22,** 548–557 (2003).
22. Mari, M. *et al.* SNX1 defines an early endosomal recycling exit for sortilin and mannose 6-phosphate receptors. *Traffic* **9,** 380–393 (2008).
23. Coudreuse, D. Y., Roel, G., Betist, M. C., Destree, O. & Korswagen, H. C. Wnt gradient formation requires retromer function in Wnt-producing cells. *Science* **312,** 921–924 (2006).
24. Prasad, B. C. & Clark, S. G. Wnt signaling establishes anteroposterior neuronal polarity and requires retromer in *C. elegans*. *Development* **133,** 1757–1766 (2006).
25. Chen, D. *et al.* Retromer is required for apoptotic cell clearance by phagocytic receptor recycling. *Science* **327,** 1261–1264 (2010).

26. Zecca, M., Basler, K. & Struhl, G. Direct and long-range action of a Wingless morphogen gradient. *Cell* **87,** 833–844 (1996).
27. Harris, J., Honigberg, L., Robinson, N. & Kenyon, C. Neuronal cell migration in *C. elegans*: regulation of Hox gene expression and cell position. *Development* **122,** 3117–3131 (1996).
28. Salser, S. J. & Kenyon, C. Activation of a *C. elegans* Antennapedia homologue in migrating cells controls their direction of migration. *Nature* **355,** 255–258 (1992).
29. Korswagen, H. C. *et al*. The Axin-like protein PRY-1 is a negative regulator of a canonical Wnt pathway in *C. elegans*. *Genes Dev.* **16,** 1291–1302 (2002).
30. Maloof, J. N., Whangbo, J., Harris, J. M., Jongeward, G. D. & Kenyon, C. A Wnt signaling pathway controls Hox gene expression and neuroblast migration in *C. elegans*. *Development* **126,** 37–49 (1999).
31. Hidalgo, A. & Ingham, P. Cell patterning in the *Drosophila* segment: spatial regulation of the segment polarity gene patched. *Development* **110,** 291–301 (1990).
32. Entchev, E. V., Schwabedissen, A. & Gonzalez-Gaitan, M. Gradient formation of the TGFβ homolog Dpp. *Cell* **103,** 981–991 (2000).
33. Teleman, A. A. & Cohen, S. M. Dpp gradient formation in the *Drosophila* wing imaginal disc. *Cell* **103,** 971–980 (2000).
34. Seaman, M. N., Harbour, M. E., Tattersall, D., Read, E. & Bright, N. Membrane recruitment of the cargo-selective retromer subcomplex is catalysed by the small GTPase Rab7 and inhibited by the Rab-GAP TBC1D5. *J. Cell Sci.* **122,** 2371–2382 (2009).
35. Rojas, R. *et al*. Regulation of retromer recruitment to endosomes by sequential action of Rab5 and Rab7. *J. Cell Biol.* **183,** 513–526 (2008).
36. Popoff, V. *et al*. Analysis of articulation between clathrin and retromer in retrograde sorting on early endosomes. *Traffic* **10,** 1868–1880 (2009).
37. Xu, Y., Hortsman, H., Seet, L., Wong, S. H. & Hong, W. SNX3 regulates endosomal function through its PX-domain-mediated interaction with PtdIns(3)P. *Nat. Cell Biol.* **3,** 658–666 (2001).
38. Skanland, S. S., Walchli, S., Brech, A. & Sandvig, K. SNX4 in complex with clathrin and dynein: implications for endosome movement. *PLoS ONE* **4,** e5935 (2009).
39. Lorenowicz, M. J. & Korswagen, H. C. Sailing with the Wnt: charting the Wnt processing and secretion route. *Exp. Cell Res.* **315,** 2683–2689 (2009).
40. Port, F. & Basler, K. Wnt trafficking: new insights into Wnt maturation, secretion and spreading. *Traffic* **11,** 1265–1271 (2010).
41. Voos, W. & Stevens, T. H. Retrieval of resident late-Golgi membrane proteins from the prevacuolar compartment of *Saccharomyces cerevisiae* is dependent on the function of Grd19p. *J. Cell Biol.* **140,** 577–590 (1998).
42. Nothwehr, S. F., Ha, S. A. & Bruinsma, P. Sorting of yeast membrane proteins into an endosome-to-Golgi pathway involves direct interaction of their cytosolic domains with Vps35p. *J. Cell Biol.* **151,** 297–310 (2000).
43. Strochlic, T. I., Setty, T. G., Sitaram, A. & Burd, C. G. Grd19/Snx3p functions as a cargo-specific adapter for retromer-dependent endocytic recycling. *J. Cell Biol.* **177,** 115–125 (2007).
44. Yu, J. W. & Lemmon, M. A. All phox homology (PX) domains from *Saccharomyces cerevisiae* specifically recognize phosphatidylinositol 3-phosphate. *J. Biol. Chem.* **276,** 44179–44184 (2001).
45. Duncan, J. R. & Kornfeld, S. Intracellular movement of two mannose 6-phosphate receptors: return to the Golgi apparatus. *J. Cell Biol.* **106,** 617–628 (1988).
46. Jin, M., Sahagian, G. G. Jr & Snider, M. D. Transport of surface mannose 6-phosphate receptor to the Golgi complex in cultured human cells. *J. Biol. Chem.* **264,** 7675–7680 (1989).
47. Lin, S. X., Mallet, W. G., Huang, A. Y. & Maxfield, F. R. Endocytosed cation-independent mannose 6-phosphate receptor traffics via the endocytic recycling compartment en route to the *trans*-Golgi network and a subpopulation of late endosomes. *Mol. Biol. Cell* **15,** 721–733 (2004).

DOI: 10.1038/ncb2281

METHODS

***C. elegans* strains and culturing.** General methods for culture, manipulation and genetics of *C. elegans* were as described[48]. Strains were cultured at 20 °C. Mutations and transgenes used in this study were: LGI, *pry-1(mu38)* (refs 29,30) and *snx-3(tm1595)*; LGII, *mab-5(e1751)* (ref. 28), *vps-35(hu68)* (ref. 23), *huSi2[Pmig-14;;mig-14::gfp]* and *muIs32[Pmec-7::gfp]* (ref. 49); LGIII, *vps-29(tm1320)* (ref. 23); LGIV, *snx-6(tm3790)* (ref. 25) and *vps-26(tm1523)* (ref. 23); LGV, *muIs35[Pmec-7::gfp]* (ref. 49); LGX, *snx-1(tm847)* (ref. 23), and unassigned, *huIs71[Pmig-14::mig-14::gfp]* (ref. 19), *muIs2[Pmab-5::LacZ]* (ref. 28), *huIs60[Pegl-20::egl-20::protA]* (ref. 23), *smIs34[Pced-1::ced-1::gfp]* (ref. 25), *huIs110[Psnx-3::snx-3::gfp]* and the extrachromosomal line *huEx149[Pegl-20::lmp-1::mcherry]* (ref. 19).

***C. elegans* phenotypes, expression constructs and transgenesis.** The final positions of the HSN and Q descendants and the polarity of the V5 seam cell division were scored in L1 larvae[27,50]. The polarity of the ALM and PLM neurons, dye filling, P12 to P11 fate transformation and *Pmab-5::lacZ* reporter gene expression were analysed as described[24,28,51]. To construct *Psnx-3::snx-3::gfp*, the *snx-3* genomic sequence and 2 kb of its promoter region were PCR amplified and cloned in frame into the *gfp* expression vector pPD95.75. A 4.4 kb upstream region of *egl-20* that specifically drives expression in the *egl-20*-producing cells[23] was used to generate *Pegl-20::snx-3::gfp* and *Pegl-20::snx-3::mcherry*. Extrachromosomal arrays were integrated as described[52].

RNAi screen in *C. elegans*. Glycerol stocks of the Ahringer RNAi library[53] were inoculated in 500 μl of Luria–Bertani medium containing 50 μg ml^{-1} ampicillin and grown overnight at 37 °C in 2.5 ml deep 96-well plates (HJ-Bioanalytik). 100 µl of bacterial culture was seeded on 3 cm nematode growth medium agar plates containing 50 μg ml^{-1} ampicillin and 1 mM isopropyl-β-D-thiogalactoside and incubated for 24 h at room temperature to induce double-stranded RNA expression. Four to eight L4-stage wild-type, *pop-1(hu9)* or *vps-29(tm1320)* animals expressing *mec-7::gfp* (*muIs32*) were added to each plate and grown at 15 °C for 72 h and then at 20 °C for 24–48 h. The final position of the Q descendants AVM and PVM was scored using a Leica MZFLIII stereomicroscope equipped with an epifluorescence unit. A minimum of 100 animals was counted on each plate. RNAi clones inducing a defect in wild type or an enhancement in one of the sensitized genetic backgrounds were retained and repeated in triplicate.

***Drosophila* stocks.** The following RNAi lines were obtained from the Vienna *Drosophila* RNAi Center (http://www.vdrc.at/): UAS-snx3^{RNAi} (104494), UAS-snx6^{RNAi} (24275) and UAS-snx6^{RNAi} (24276). Note that UAS-snx3^{RNAi} (34166) gives a similar but weaker phenotype than UAS-snx3^{RNAi} (104494) (data not shown). The Gal4-driver lines used are indicated in the figure legend and are available from the Bloomington *Drosophila* Stock Center (BDSC). The P-element line yw;;P{EPgy2}CG6359^{EY05688} (stock no 16668) was obtained from the BDSC and the P element was recombined with ywhsp-Flp;sp/cyo;FRT82/Tm6b to generate ywhsp-Flp;sp/cyo;FRT82 CG6359^{EY05688}/Tmb6. Clones were generated by crossing flies to ywhsp-Flp;;FRT82 ubiGFP and the F1 progeny was heat shocked 42 h after egg laying for 45 min at 37 °C.

***Drosophila* immunostaining.** Immuno-staining was carried out using standard protocols. Briefly, third-instar larvae were dissected in ice-cold Ringer's solution. Discs were fixed and permeabilized in PBS containing 4% paraformaldehyde and 0.05% Triton X-100 for 25 min at room temperature. Discs were washed in PBS containing 0.05% Triton X-100 (PBT) for 1 h at room temperature and then incubated in primary antibody solution at 4 °C overnight. Afterwards, discs were washed in PBT containing 1% goat serum for 1 h at room temperature and subsequently incubated in secondary antibody solution for 2 h at room temperature. After a final wash for 1 h in PBT, discs were mounted on coverslips using double-sided tape as a spacer to avoid compression of the discs. Antibodies were diluted in PBT. The extracellular Wg staining was carried out as described[54]. Images were collected on a Zeiss LSM710 or Leica SP5 confocal microscope using the sequential scanning mode. Images were analysed using ImageJ (NIH).

Cell culture, transfection, immunofluorescence and western blot analysis. HeLa cells were maintained in RPMI 1640 medium (GIBCO) containing 10% heat-inactivated FCS (GIBCO), 2 mM gluta-MAX, 100 U ml^{-1} penicillin and 100 μg ml^{-1} streptomycin. HeLa cells were transfected with control siRNA (Dharmacon), *RAB7* siRNA (ref. 55) or SMART pooled siRNAs against *SNX3* (M-011521-01-0010) or *SNX12* (M-013648-00) (Dharmacon) using Oligofectamine (Invitrogen). Cells were transfected two times with a 48 h interval between transfections and were analysed by immunofluorescence or western blotting 24 h after the last transfection. The plasmid containing human Wls–mCherry (1 µg) and plasmids containing human SNX3-GFP and SNX12-GFP (1 µg) were transfected using FuGENE transfection reagent (Roche) 24 h and 8 h before further analyses, respectively. Human *Wls* complementary DNA was cloned in frame with mCherry into the pcDNA3.1zeo vector (Invitrogen). Human *SNX3* and *SNX12* cDNA were cloned into the pEGFP-N3, the pEGFP-C1 or the pEGFP-C2 vector (Clonetech). GFP–SNX3 was cloned into the vector XLG3 for lentiviral expression.

For immunofluorescence analysis, HeLa cells were plated on glass coverslips, fixed in 0.1 M phosphate buffer containing 4% paraformaldehyde for 10 min on ice and permeabilized with 0.1% Triton X-100 for 5 min, except for LAMP1 localization, for which 0.1% (w/v) saponin was used for permeabilization. Thereafter, cells were incubated with 0.5% BSA for 30 min followed by incubation with the indicated primary antibodies and subsequent incubation with a chicken-anti-mouse-Ig or chicken-anti-rabbit-Ig antibody labelled with Alexa 488 (Molecular Probes). For nuclear staining DAPI was used. Images were recorded on a Leica SPE or a Leica AOBS-SP2 confocal microscope. Co-localization analysis was carried out using the ICA plug-in from ImageJ (NIH), or by using Volocity co-localization software (Perkin Elmer). Volume integration of voxel intensity was calculated using the Pearson's coefficient, measuring the protein of interest relative to a marker. Thresholds were set independently for each channel.

For western blot analysis, cells were lysed in Laemmli sample buffer and cell lysates were separated on 10% SDS–polyacrylamide gel electrophoresis gels, transferred onto polyvinylidene difluoride membranes (Bio-Rad) and stained with antibodies against the indicated proteins. Cell fractionation samples were prepared as described[34]. To quantify MIG-14::GFP protein levels, synchronized L1 larvae were lysed in four volumes of 25 mM Tris (pH 7.5), 150 mM NaCl, 0.5 mM $CaCl_2$ and 1% TX-114 supplemented with protease inhibitors (Roche). Densitometric analysis was carried out on scanned images using ImageJ (NIH).

GFP nanotrap. Culture dishes (15 cm) with HeLa cells at approximately 95% confluency were washed twice with ice-cold PBS and lysed by the addition of lysis buffer containing 0.1 M MES–NaOH at pH 6.5, 1 mM Mg acetate, 0.5 mM EGTA, 200 µM sodium vanadate, 1% (w/v) digitonin and protease inhibitors. After scraping, lysates were cleared by centrifugation at 13,000 *g* for 10 min at 4 °C. Cell lysates were added to 30 µl of equilibrated GFP-Trap beads (ChromoTek) followed by incubation with gentle end-over-end mixing for 1 h at 4 °C. Beads were then spun down at 2,000 *g* for 2 min at 4 °C and washed three times in detergent-free lysis buffer. Complexes were eluted from the GFP-Trap beads by boiling in NuPAGE LDS sample buffer (Invitrogen) and subjected to gel electrophoresis and western blotting.

Electron microscopy. Cryo-immuno-electron microscopy was carried out as described[22]. HeLa cells expressing GFP–SNX3 and mCherry–VPS26 were fixed in 4% (w/v) paraformaldehyde, 0.05% (w/v) glutaraldehyde in 0.1 M phosphate buffer. The fixed cells were scraped off the dish in 1% gelatine in phosphate buffer and spun down in 10% gelatine. After 1 h of solidification on ice, pellets were cut into small blocks and infiltrated with 2.3 M sucrose at 4 °C overnight. The blocks were mounted on aluminium pins and frozen in liquid nitrogen for ultrathin cryosectioning. Sections (70 nm) were collected at −120 °C in 1% methylcellulose in 1.2 M sucrose on formvar/carbon-coated copper mesh grids. The sections were labelled with polyclonal goat anti-GFP (Rockland Immunochemicals) and polyclonal rabbit anti-RFP (red fluorescent protein, Molecular Probes Invitrogen) antibodies and anti-goat 10 nm gold and anti-rabbit 6 nm gold secondary antibodies (Aurion). The sections were counterstained with 0.3% (w/v) uranyl acetate in 1.8% (w/v) methylcellulose and imaged on an FEI Tecnai 12 Biotwin transmission electron microscope equipped with a bottom mount.

Statistical analysis. In each graph, data represent mean ± standard deviation or mean ± s.e.m. (see figure legends) of the indicated number (n) of independent experiments. Results were compared with control experiments using a Student's t-test. Pearson's coefficients were calculated using the ICA plug-in for ImageJ (NIH) or by using Velocity co-localization software (Perkin Elmer) as described[56].

Antibodies. The following antibodies were used in this study: polyclonal antibody against *Drosophila* Wls (1:1,500; ref. 18); polyclonal chicken anti-Wls (1:3,000, Abcam); polyclonal rabbit anti-SNX3 (1:500, Abcam); polyclonal goat antibody recognizing both SNX3 and SNX12 (1:500, C16, Santa Cruz); polyclonal goat anti-SNX5 (1:1,000, D18, Santa Cruz); polyclonal goat anti-EEA1 (1:200, N19, Santa Cruz); monoclonal mouse anti-EEA1 (1:25, BD Transduction Laboratories); monoclonal mouse anti-tubulin (1:5,000, clone DM1A, Sigma-Aldrich); monoclonal mouse anti-GFP (1:3,000, mix of clones 7.1 and 13.1, Roche); monoclonal mouse anti-GFP (1:5,000, Clonetech); monoclonal mouse anti-SNX1 (1:500, clone 51, BD Transduction Laboratories); monoclonal mouse anti-Wg (1:1,000, 4D4; DSHB); mouse monoclonal anti-LAMP1 (1:1,000) (DSHB); chicken-anti-mouse-Ig or chicken-anti-rabbit-Ig antibody labelled with Alexa 488 or goat anti-mouse Alexa 594 (Molecular Probes), rabbit anti-goat and goat anti-rabbit Cy5 (Jackson Immunoresearch Laboratories). The following antibodies were provided by other researchers: polyclonal rabbit anti-LAMP1 (1:1,000, 270C) from A. Toye; polyclonal rabbit anti-hVps26 (1:1,000 WB; 1:100 IF) and anti-hVps35 (1:2,000) from M. Seaman; polyclonal guinea-pig anti-Sens (1:500, GP55) from H. Bellen;

polyclonal rabbit anti-Hh (1:500) from S. Eaton and polyclonal rabbit anti-pMad (1:1,000) from G. Morata.

48. Lewis, J. A. & Fleming, J. T. Basic culture methods. *Methods Cell Biol.* **48,** 3–29 (1995).
49. Ch'ng, Q. *et al.* Identification of genes that regulate a left-right asymmetric neuronal migration in *Caenorhabditis elegans*. *Genetics* **164,** 1355–1367 (2003).
50. Whangbo, J., Harris, J. & Kenyon, C. Multiple levels of regulation specify the polarity of an asymmetric cell division in *C. elegans*. *Development* **127,** 4587–4598 (2000).
51. Herman, M. A. & Horvitz, H. R. The *Caenorhabditis elegans* gene *lin-44* controls the polarity of asymmetric cell divisions. *Development* **120,** 1035–1047 (1994).
52. Mello, C. C. & Fire, A. in *Caenorhabditis elegans: Modern biological analysis of an organism*, Vol. 48 (eds Epstein, H. F. & Shakes, D. C.) 451–482 (Academic, 1995).
53. Kamath, R. S. *et al.* Systematic functional analysis of the *Caenorhabditis elegans* genome using RNAi. *Nature* **421,** 231–237 (2003).
54. Baeg, G. H., Lin, X., Khare, N., Baumgartner, S. & Perrimon, N. Heparan sulfate proteoglycans are critical for the organization of the extracellular distribution of Wingless. *Development* **128,** 87–94 (2001).
55. Kawakami, A. *et al.* Rab7 regulates maturation of melanosomal matrix protein gp100/Pmel17/Silv. *J. Invest. Dermatol.* **128,** 143–150 (2008).
56. Bolte, S. & Cordelieres, F. P. A guided tour into subcellular colocalization analysis in light microscopy. *J. Microsc.* **224,** 213–232 (2006).

nature cell biology

DOI: 10.1038/ncb2281

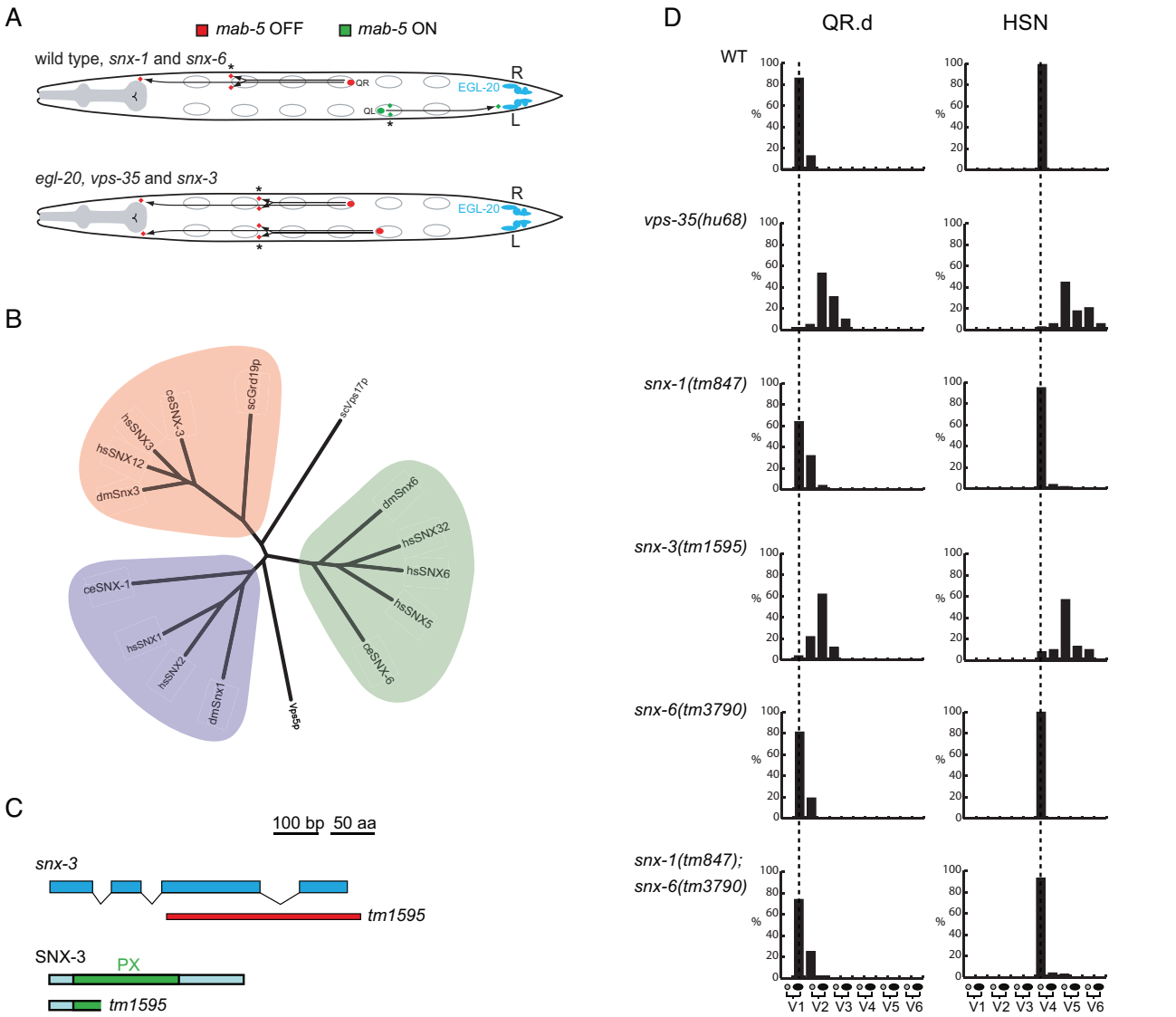

Figure S1 (**A**) Schematic representation of Q.d migration. Dorsal view, anterior is to the left. Cells are in green or red when *mab-5* expression is activated or absent, respectively. The *egl-20* (Wnt) expressing cells are indicated in blue. Grey circles indicate the position of the seam cells V1 to V6. The final positions of the Q.paa and Q.pap cells in wild type and *egl-20*, *vps-35* and *snx-3* mutants are indicated by an asterisk. (**B**) Phylogenetic tree of yeast (sc), *C. elegans* (ce), *Drosophila* (dm) and human (hs) SNX-BAR (green and purple) and SNX3 (pink) related sorting nexins. Phylogenetic analysis was performed using CLUSTALW (default program parameters). (**C**) Schematic representation of the deleted region in *snx-3(tm1595)*. The Phox-homology (PX) domain is shown in green. *snx-3(tm1595)* is a combined insertion and deletion allele that removes 420 base pairs and inserts 14 base pairs (inserted sequence is TTCTCCGAAAAATC). (**D**) The final positions of QR.paa and QR.pap and the HSN neurons are indicated relative to the invariant positions of the seam cells V1 to V6 (n>50).

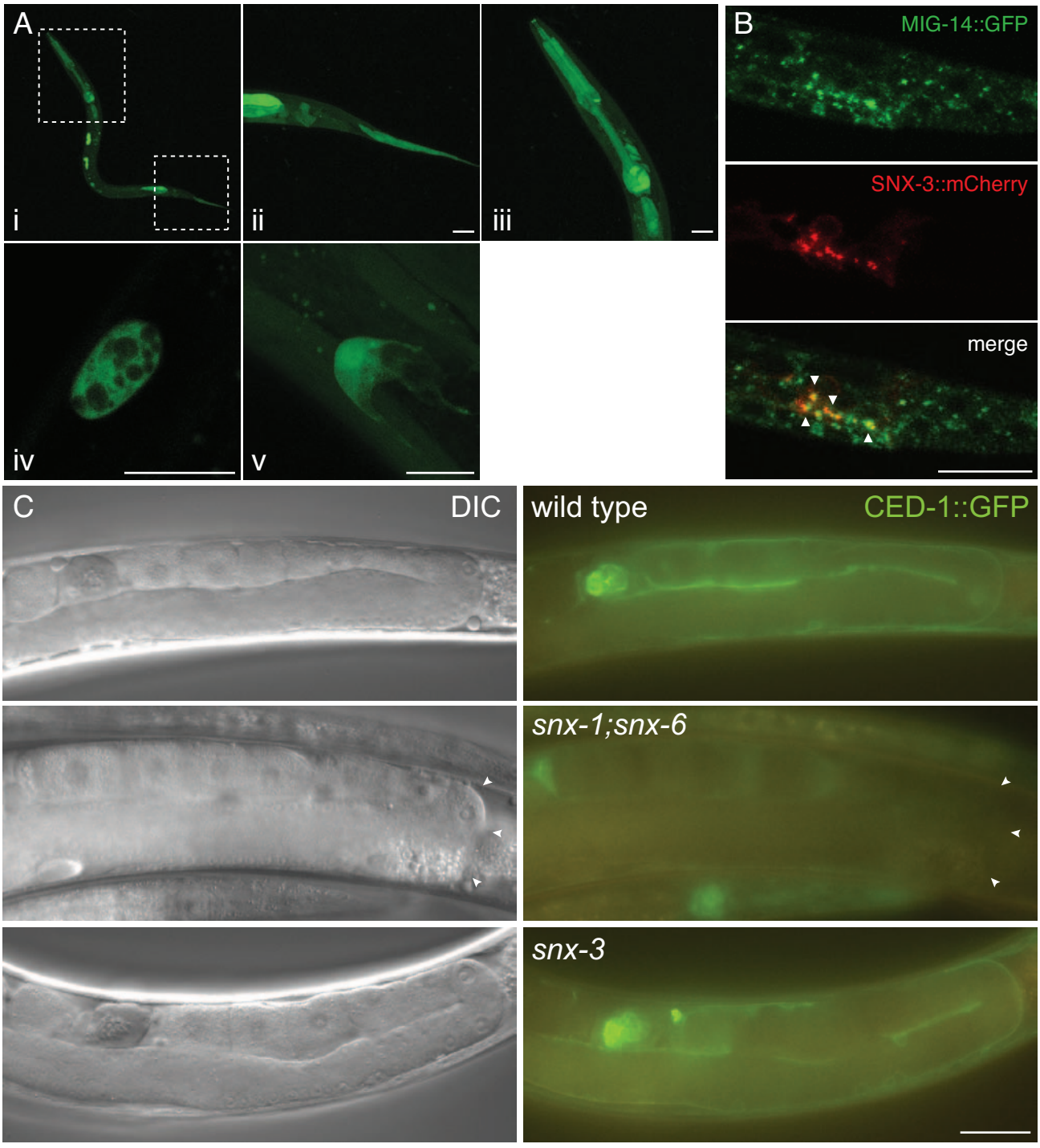

Figure S2 (**A**) Expression pattern of a fusion of the *snx-3* promoter and coding sequence to *gfp* (*huIs110*). *snx-3* is ubiquitously expressed (**i**), with most prominent expression in the tail hypodermis and rectal epithelial cells (including the EGL-20 producing cells) (**ii**), the pharynx (**iii**), coelomocytes (**iv**) and the distal tip cells (**v**). Scale bars 10 μm. (**B**) Co-localization of MIG-14::GFP (green) and SNX-3::mCherry (red) in EGL-20 producing cells in *C. elegans*. Confocal images of the *Pmig-14::mig-14::gfp* expressing transgene *huSi2* combined with the *Pegl-20::snx-3::mcherry* expressing transgene *huEx221*. Arrowheads indicate examples of co-localization. Images are projections of several confocal sections. Scale bar 10 μm. (**C**) CED-1::GFP levels in the gonadal sheath cell are strongly reduced in *snx-1; snx-6* double mutants. CED-1::GFP was expressed using the *smIs34* transgene[1]. CED-1::GFP levels are not reduced in *snx-3* mutants. Consistently, *snx-3* RNAi does not induce defects in cell corpse engulfment[1]. Scale bar 50 μm.

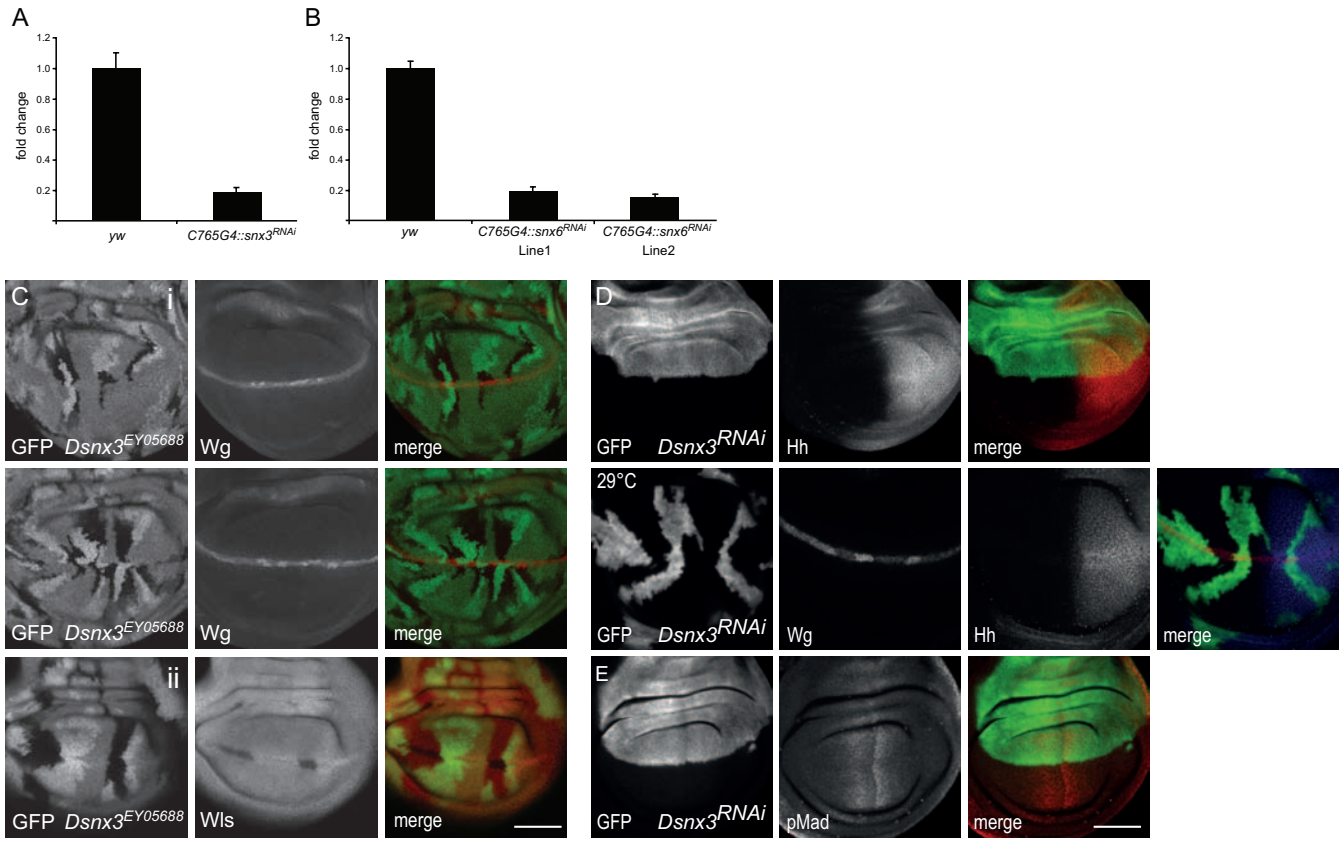

Figure S3 (**A**, **B**) Efficient knock-down of *Dsnx3* and *Dsnx6* transcript upon RNAi. Imaginal discs from third instar larvae were analyzed by qt-RT-PCR. Total RNA was extracted from 16 wing imaginal discs from each genotype using the Nucleospin RNA II kit (Macherey-Nagel). Quantitative PCR reactions were performed in triplicates and monitored using the Applied Biosystems SYBR Green kit and the ABI Prism 7900HT System (Applied Biosystems). All results were simultaneously normalized to Actin5C, tubulin-1a and TBP mRNA levels and the expression levels calculated using the ddCt method (Applied Biosystems user bulletin #2, updated version 04/2001). Relative change of mRNA abundance relative to wild type imaginal discs (yw) is shown. Error bars represent standard deviation. RNAi Lines from VDRC Vienna are as follows: *snx3* CG6359 TF 104494; *snx6* Line1 CG8282 TF 24275; *snx6* Line2 CG8282 TF 24276. (**C**) Homozygous clones of $Dsnx3^{EY05688}$ accumulate Wg and loose WIs in Wnt producing cells. (**i**) Wg levels (red) are elevated in homozygous $Dsnx3^{EY05688}$ clones, which are marked by the absence of GFP expression (green). (**ii**) $Dsnx3^{EY05688}$ clones loose WIs protein (red) specifically in Wg producing cells. Clones are marked by the absence of GFP. (**D**, **E**) Reduction of *Dsnx3* expression does not interfere with Hh secretion or Dpp signaling. (**D**) *Dsnx3* was knocked-down by expressing the corresponding UAS-hairpin with *apGal4* in the dorsal compartment of the wing imaginal disc. The expression domain is marked by a *UAS-CD8GFP* transgene (green). Hh protein levels (red) are similar in the dorsal and ventral compartments (upper panel). $Dsnx3^{RNAi}$ was expressed in clones of cells using an *hsp-FLP;;act>y>Gal4* driver line and appropriate heat shock conditions (green). $Dsnx3^{RNAi}$ clones accumulate Wg (red) in producing cells, but leave Hh protein levels (blue) unaffected (lower panel). (**E**) Dpp dependent phosphorylation of Mad (red) is not altered when *Dsnx3* is knocked-down by expression with *apGal4*. Scale bars, 50 μm.

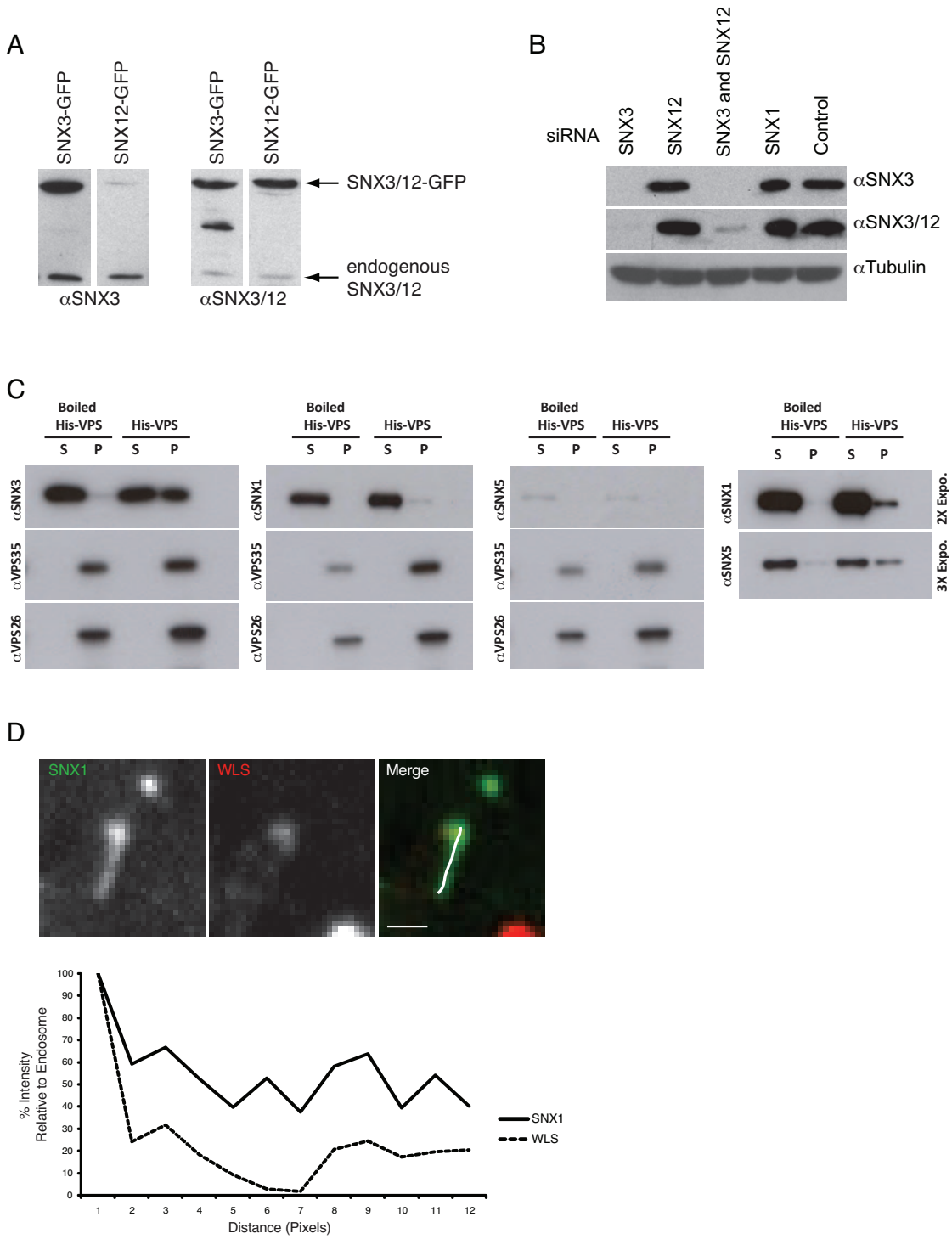

Figure S4 Western blot detection of SNX3 and SNX12 in HeLa cells. (**A**) Cells were transfected with SNX3-GFP or SNX12-GFP and Western blots were stained with a polyclonal rabbit anti-SNX3 antibody (Abcam) or a polyclonal goat antibody recognizing both SNX3 and SNX12 (C16, Santa Cruz). (**B**) Cells were treated with control, SNX3, SNX12 or SNX1 siRNA and SNX3 and SNX12 were detected using the SNX3 specific antibody or the antibody that recognizes both SNX3 and SNX12. Note that SNX3 and SNX12 are of similar size and are therefore not separated. (**C**) SNX3 directly associates with the cargo-selective sub-complex of the retromer. 3xFLAG-VPS26-VPS29-VPS35-His_6 trimeric complex (His-VPS) was isolated from BL21 *E. coli* onto TALON resin and incubated with 2 μM of either recombinant SNX3, SNX1 or SNX5 for 2 hours at 4ºC. Supernatant (S) and TALON containing resin (P) were isolated prior to Western analysis. SNX3 directly associates with His-VPS, as do SNX1 and SNX5, although this is less well pronounced (longer exposures are shown). Control: boiled His-VPS resin. (**D**) Quantification of GFP-SNX1 (green) and Wls-mCherry (red) in an endosome and the tubule that is projecting from it. Scale bar is 4 μm.

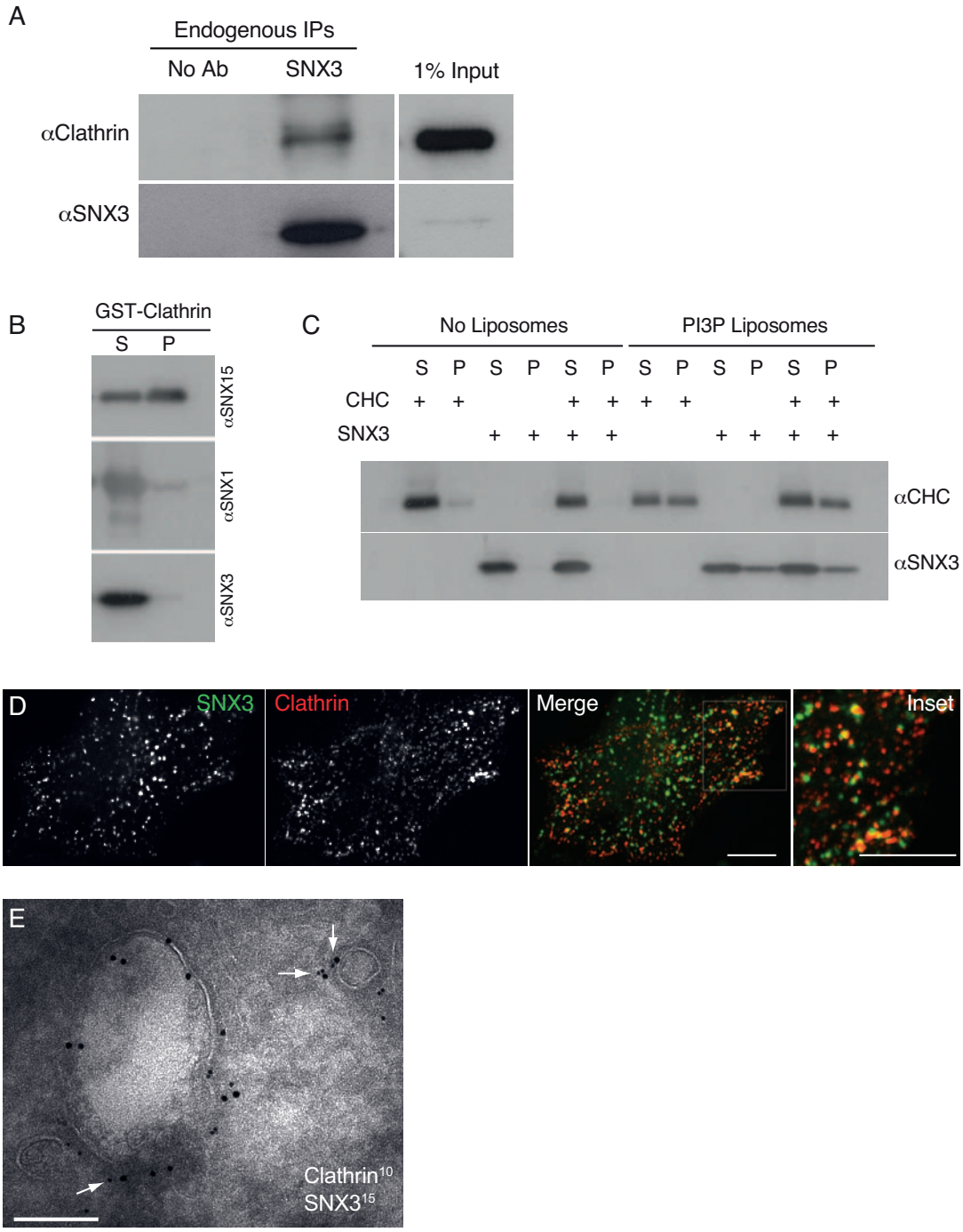

Figure S5 SNX3 associates indirectly with clathrin. (**A**) Immunoprecipitation of endogenous SNX3 reveals an association with clathrin heavy chain. Cell extracts from HeLa cells were incubated with anti-SNX3 antibody prior to western analysis. Control, no antibody. (**B**) Purified recombinant GST-clathrin (residues 1-579) was isolated from BL21 *E. coli* onto glutathione resin and incubated with 5 μM of purified recombinant SNX3, SNX1 or as a positive control SNX15 (a sorting nexin that directly associates with clathrin, C. Danson, and P.J. Cullen, unpublished). After centrifugation, supernatant (S) and glutathione resin containing pellet (P) were resolved prior to western analysis with anti-SNX3, anti-SNX1 or anti-SNX15 antibodies. (**C**) To determine whether PI(3)P-mediated membrane association is required for the direct binding of SNX3 with clathrin, the interaction of 20 μM clathrin heavy chain (cleaved from purified recombinant GST-clathrin (residues 1-579) with 5 μM recombinant SNX3 was performed on artificial liposomes supplemented with 1 molar percent PI(3)P (control - no liposomes to verify that association is lipid dependent). After separation of supernatant (S) from pellet (P), western blotting revealed that the binding of SNX3 to PI(3)P-containing liposomes did not enhance, above basal level, the liposome association of clathrin. This is consistent with clathrin not binding directly to SNX3 even after engagement with PI(3)P-containing liposomes. (**D**) Partial co-localization between GFP-SNX3 (green) and dsRed-clathrin light chain (red) in HeLa cells. Imaging was performed in live cells with a single selected frame being shown (Pearson's correlation is 0.10 ± 0.03; data are represented as mean ± SD, n=30 cells). Scale bar, 30 μm. (**E**) Immuno-electron microscopy of GFP-SNX3 (15 nm gold) and endogenous clathrin heavy chain (10 nm gold) in HeLa cells. Scale bar, 200 nm.

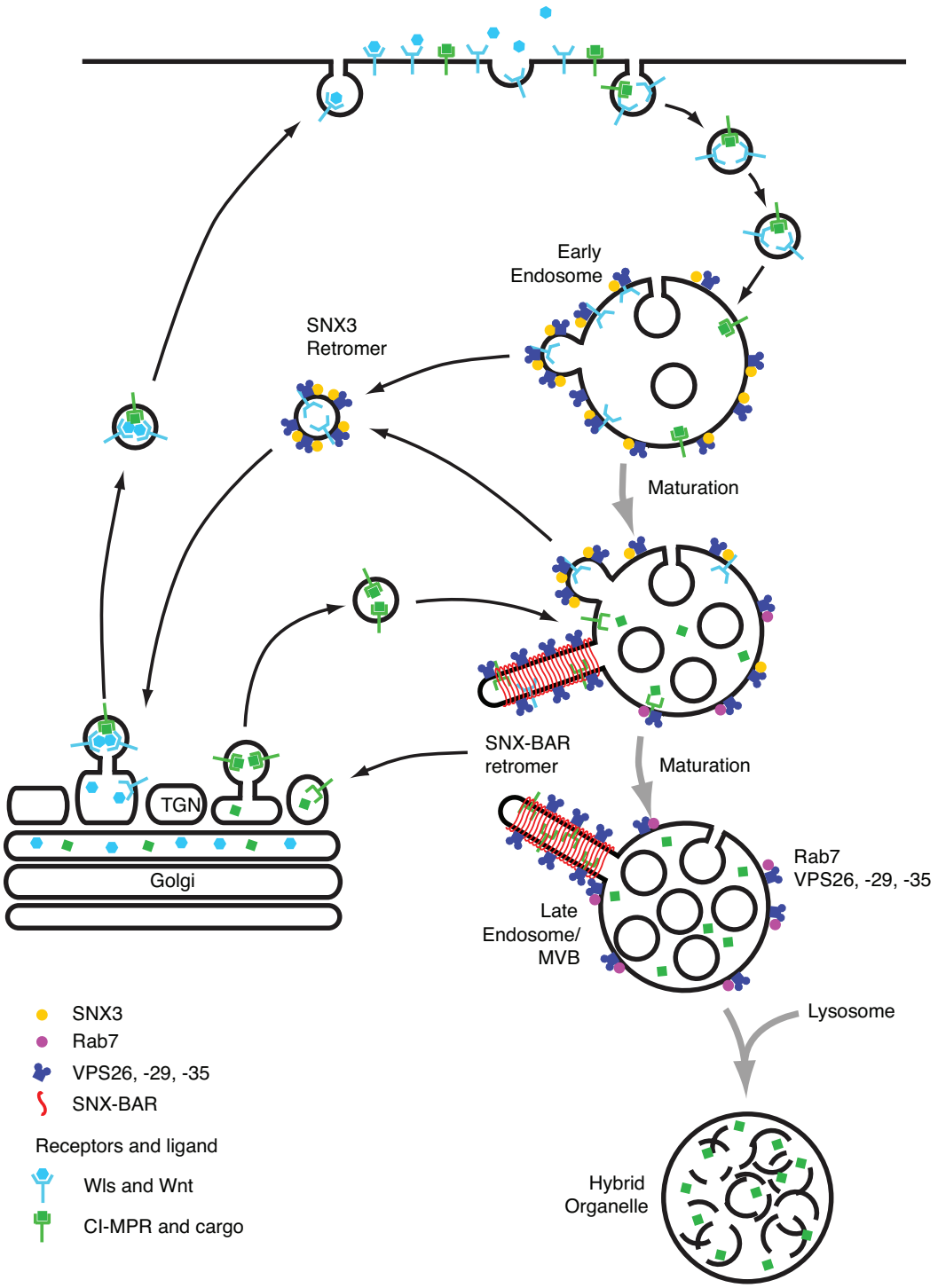

Figure S6 A model describing the spatial segregation of SNX3 retromer and SNX-BAR retromer along the endosomal maturation pathway. The SNX3 retromer mediates endosome to TGN retrieval of endocytosed Wls from early endosomes through a vesicular trafficking mechanism. The SNX-BAR retromer retrieves cargo proteins such as the CI-MPR from endosomes that are at the early to late transition point in the endosomal maturation pathway and acts through a tubular endosomal sorting mechanism. For simplicity, the multi-pass transmembrane protein Wls and the single-pass transmembrane protein CI-MPR are drawn similarly.

Fig. 1E

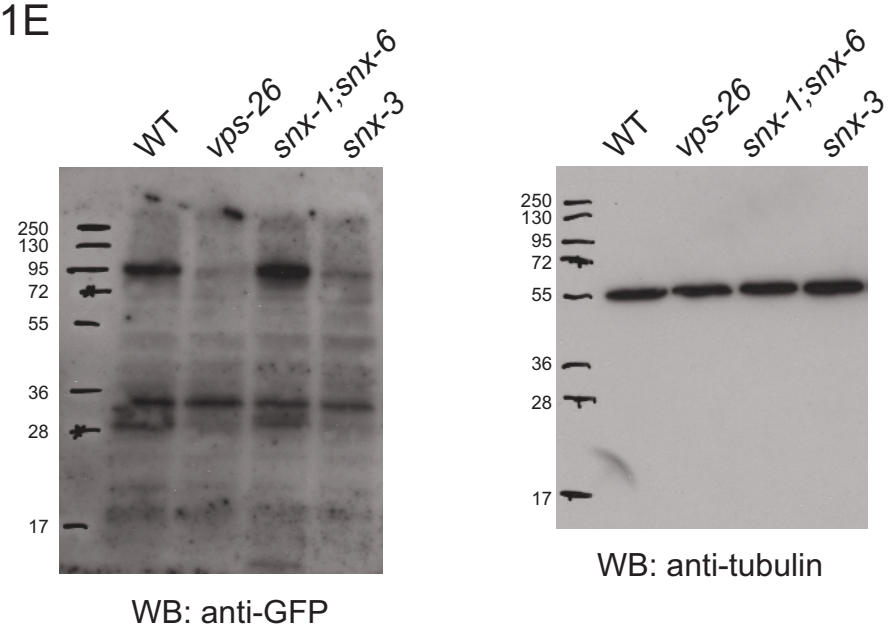

Figure S7 Full scans

Fig. 3C

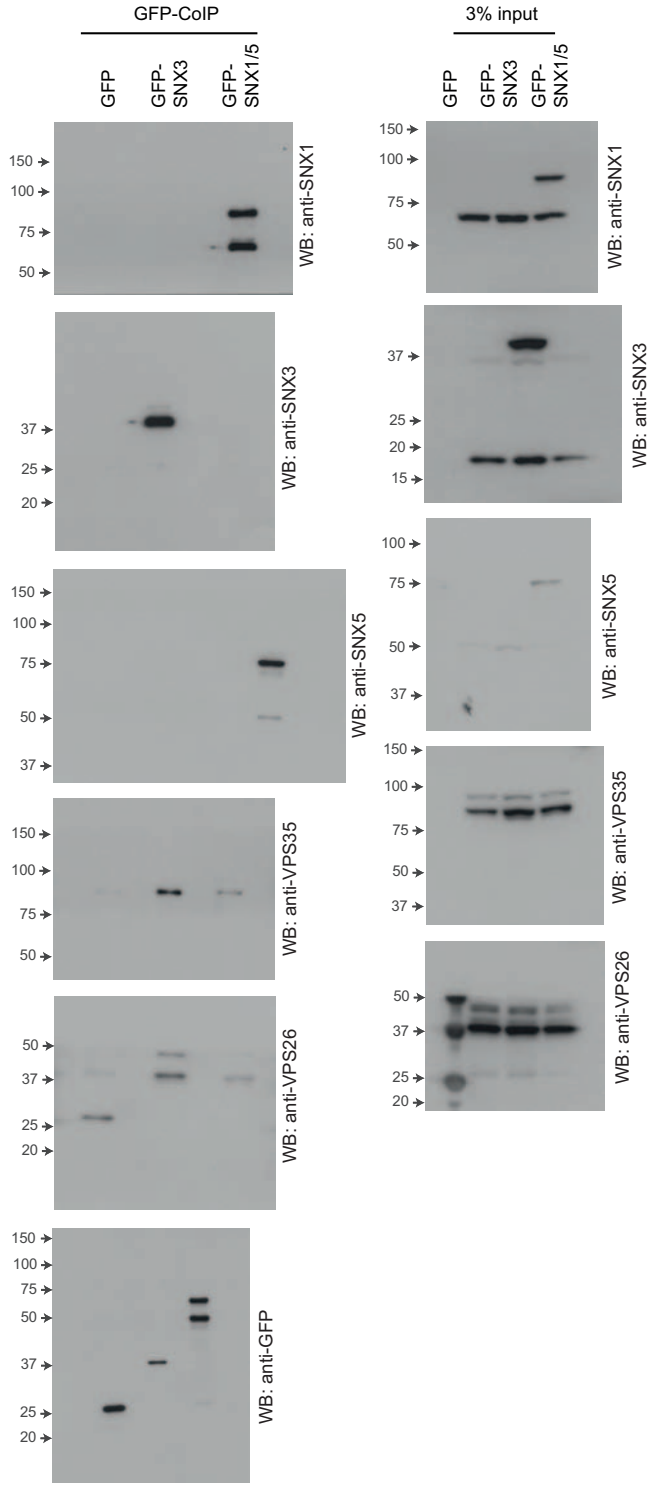

Fig. 3D

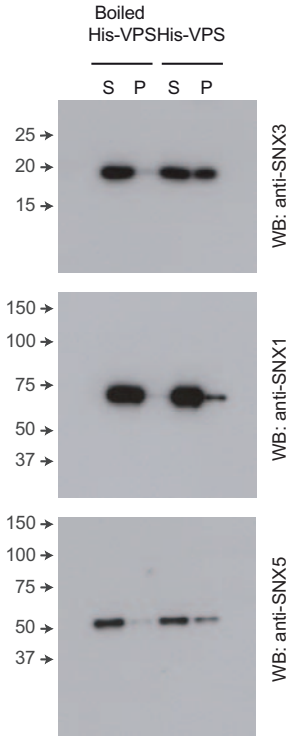

Figure S7 continued Full scans

Fig. 4C

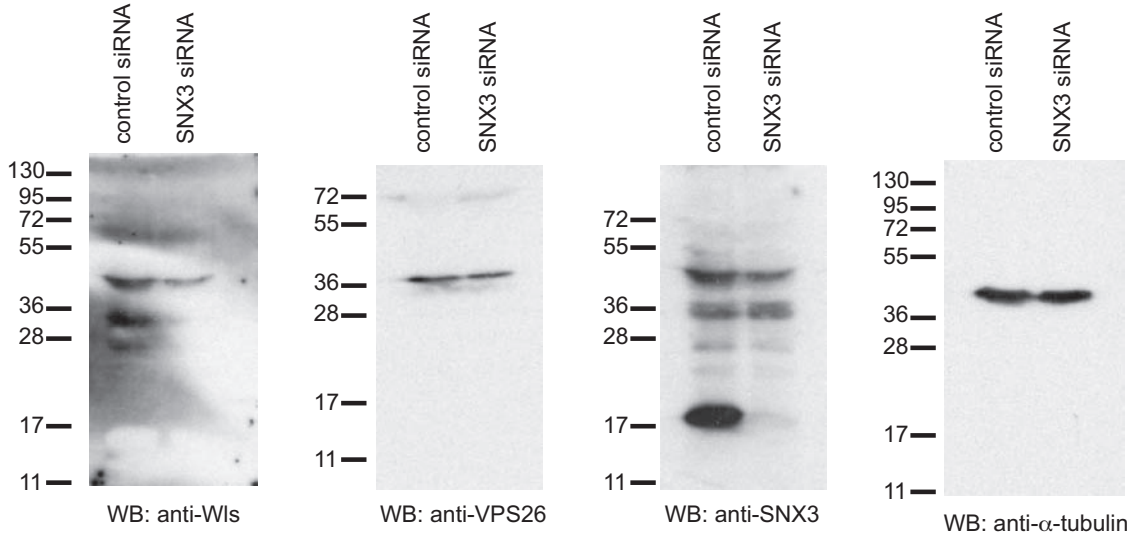

Fig. 4D

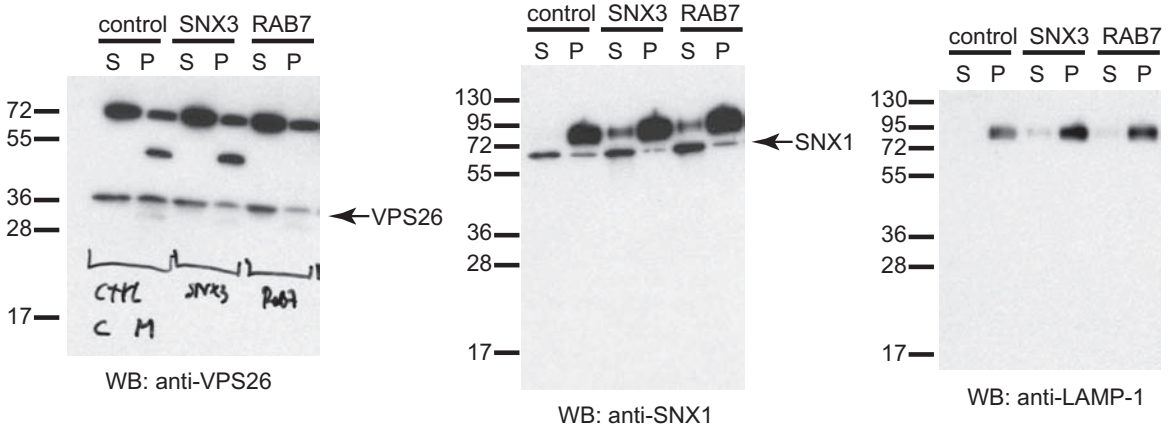

Figure S7 continued Full scans

Supplementary Table legends

Table S3. A genome-wide RNAi screen for genes that affect the EGL-20 (Wnt) dependent migration of the QL descendants
To identify novel genes required for the EGL-20 dependent posterior migration of the QL neuroblast descendants, a genome-wide RNAi screen was performed using the Ahringer RNAi library[2]. To rapidly score the final position of the QL descendants, QL.paa (PVM) was visualized using a *mec-7::gfp* reporter[3]. To sensitize the screen for defects in EGL-20 signaling, a hypomorphic allele of the TCF transcription factor *pop-1* and a null allele of *vps-29* (a retromer subunit that is only partially required for endosome to TGN recycling of MIG-14 (Wls) and EGL-20 secretion[4]) were used. In both genetic backgrounds, EGL-20 signaling is reduced, resulting in a partially penetrant defect in the posterior migration of the QL.d (in 18 ± 5% of *pop-1(hu9)* animals and in 30 ± 5% of *vps-29(tm1320)* animals on control RNAi, the QL.d localize anterior to the vulva). Treatment of *pop-1(hu9)* or *vps-29(tm1320)* with *vps-35* RNAi induced a >3-fold enhancement of this phenotype over control RNAi[5], validating the approach of our screen. Each positive RNAi clone identified in the screen was retested in triplicate in the three genetic backgrounds (gene specific RNAi column, data represented as the mean of three independent experiments, n numbers indicated on the right). In each case, empty vector RNAi was taken along as a control (control RNAi column, n numbers indicated on the right). An RNAi result was retained when knock down induced a defect in wild type or an enhancement of at least two-fold over control RNAi in one of the sensitized genetic backgrounds.

References

1. Chen, D. *et al.* Retromer is required for apoptotic cell clearance by phagocytic receptor recycling. *Science* **327**, 1261-1264 (2010).
2. Kamath, R.S. *et al.* Systematic functional analysis of the *Caenorhabditis elegans* genome using RNAi. *Nature* **421**, 231-237 (2003).
3. Ch'ng, Q. *et al.* Identification of genes that regulate a left-right asymmetric neuronal migration in *Caenorhabditis elegans*. *Genetics* **164**, 1355-1367 (2003).
4. Yang, P.T. *et al.* Wnt signaling requires retromer-dependent recycling of MIG-14/Wntless in Wnt-producing cells. *Dev Cell* **14**, 140-147 (2008).
5. Coudreuse, D.Y., Roel, G., Betist, M.C., Destree, O. & Korswagen, H.C. Wnt gradient formation requires retromer function in Wnt-producing cells. *Science* **312**, 921-924 (2006).

Table S1. Wnt signaling phenotypes of retromer and sorting nexin mutants

	WT	*vps-35(hu68)*	*snx-3(tm1595)*	*snx-1(tm847); snx-6(tm3790)*
QL.d migration	0	100	100	0
QR.d migration	1	98	74	2
HSN	1	97	92	7
ALM polarity	0	21	53	0
PLM polarity	0	29	57	0
P12 to P11	0	6	0	0
T polarity	1	12	2	1
V5 polarity	0	32	6	0
Embryonic lethal	2	n.d.	1	4

Numbers indicate percentage defective (n>100). The final positions of QL.paa (PVM) and QR.paa (AVM) was scored using Nomarski optics and the polarity of the ALM and PLM mechanosensory neurons was scored using *a mec-7::gfp (muIs32 or muIs35)* expressing transgene. The final position of the HSN neurons, the polarity of the V5 division and P12 to P11 fate transformation were scored using Nomarski microscopy at the appropriate developmental stage. T cell polarity was scored by DiO filling of the T derived phasmid structure in young adults.

Table S2. Rescue of the *snx-3(tm1595)* QL.d migration defect

	% QL.d in posterior	n
WT	100	112
snx-3(tm1595)	0	>200
mab-5(e1751)gf	100	110
snx-3(tm1595); mab-5(e1751)gf	100	114
pry-1(mu38)	100	103
snx-3(tm1595); pry-1(mu38)	78	105
snx-3(tm1595); Pegl-20::snx-3::gfp	54	263
snx-3(tm1595); Pegl-20::snx-1::gfp	0	141
snx-3(tm1595); Pmig-14::mig-14::gfp	100	50

The final position of QL.paa (PVM) was scored as anterior or posterior to the vulva in young adult hermaphrodites using a *mec-7::gfp (muIs32)* reporter transgene or using Nomarski optics.